

# Effect of Calcium on the Oxidative Phosphorylation Cascade in Skeletal Muscle Mitochondria

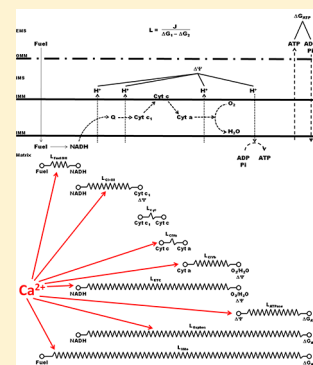
Brian Glancy,<sup>\*,†</sup> Wayne T. Willis,<sup>‡</sup> David J. Chess,<sup>†</sup> and Robert S. Balaban<sup>†</sup>

<sup>†</sup>Laboratory of Cardiac Energetics, National Heart, Lung and Blood Institute, National Institutes of Health, Bethesda, Maryland 20892, United States

<sup>‡</sup>School of Life Sciences, Arizona State University, Tempe, Arizona 85287, United States

## S Supporting Information

**ABSTRACT:** Calcium is believed to regulate mitochondrial oxidative phosphorylation, thereby contributing to the maintenance of cellular energy homeostasis. Skeletal muscle, with an energy conversion dynamic range of up to 100-fold, is an extreme case for evaluating the cellular balance of ATP production and consumption. This study examined the role of  $\text{Ca}^{2+}$  in the entire oxidative phosphorylation reaction network in isolated skeletal muscle mitochondria and attempted to extrapolate these results back to the muscle, *in vivo*. Kinetic analysis was conducted to evaluate the dose–response effect of  $\text{Ca}^{2+}$  on the maximal velocity of oxidative phosphorylation ( $V_{\text{maxO}}$ ) and the ADP affinity. Force-flow analysis evaluated the interplay between energetic driving forces and flux to determine the conductance, or effective activity, of individual steps within oxidative phosphorylation. Measured driving forces [extramitochondrial phosphorylation potential ( $\Delta G_{\text{ATP}}$ ), membrane potential, and redox states of NADH and cytochromes  $b_{\text{H}}$ ,  $b_{\text{L}}$ ,  $c_1$ ,  $c$ , and  $a, a_3$ ] were compared with flux (oxygen consumption) at 37 °C; 840 nM  $\text{Ca}^{2+}$  generated an ~2-fold increase in  $V_{\text{maxO}}$  with no change in ADP affinity (~43  $\mu\text{M}$ ). Force-flow analysis revealed that  $\text{Ca}^{2+}$  activation of  $V_{\text{maxO}}$  was distributed throughout the oxidative phosphorylation reaction sequence. Specifically,  $\text{Ca}^{2+}$  increased the conductance of Complex IV (2.3-fold), Complexes I and III (2.2-fold), ATP production/transport (2.4-fold), and fuel transport/dehydrogenases (1.7-fold). These data support the notion that  $\text{Ca}^{2+}$  activates the entire muscle oxidative phosphorylation cascade, while extrapolation of these data to the exercising muscle predicts a significant role of  $\text{Ca}^{2+}$  in maintaining cellular energy homeostasis.



Exercise presents a severe challenge to energetic homeostasis in skeletal muscle as tissue-specific oxygen consumption rates can increase over 100-fold from rest to maximal aerobic exercise.<sup>1</sup> Increases in skeletal muscle work rate are associated with modest decreases in the cytosolic ATP free energy ( $\Delta G_{\text{ATP}}$ ) primarily through increases in ADP concentration and  $\text{P}_i$  concentration.<sup>2–4</sup> Because both muscle contraction and ion transport processes are dependent on  $\Delta G_{\text{ATP}}$ , minimizing the reduction in  $\Delta G_{\text{ATP}}$  during increases in energy demand is critical to the maintenance of normal cellular functions, such as ion gradients for signaling, as well as allowing peak muscle performance. The release of calcium ( $\text{Ca}^{2+}$ ) from the sarcoplasmic reticulum (SR) and subsequent binding to troponin C allows muscle contraction and the associated utilization of energy to occur, while influx of  $\text{Ca}^{2+}$  into mitochondria has been shown to result in increased energy conversion potential.<sup>5–9</sup> This balanced activation of both energy conversion and utilization pathways has been proposed to play a key role in the maintenance of energetic homeostasis in contracting muscle.<sup>10–13</sup>

$\text{Ca}^{2+}$  has long been known to stimulate flux through the citric acid cycle by activation of pyruvate, isocitrate, and 2-oxoglutarate dehydrogenases.<sup>14</sup> More recently,  $\text{Ca}^{2+}$  has also been shown to directly stimulate ATP production through activation of the  $\text{F}_1\text{F}_0$ -ATP synthase,<sup>9</sup> and flux through

Complex III of the electron transport chain (ETC) may also be stimulated by  $\text{Ca}^{2+}$ .<sup>15</sup> Despite the importance of  $\text{Ca}^{2+}$  for both skeletal muscle contraction and activation of oxidative phosphorylation, few studies have examined the effects of  $\text{Ca}^{2+}$  on skeletal muscle mitochondrial energy conversion. Martin et al.<sup>16</sup> found that an increasing level of  $\text{Ca}^{2+}$  lowered the respiratory control (RCR) and ADP/O ratios in isolated skeletal muscle mitochondria, though the free  $\text{Ca}^{2+}$  concentrations used in that study (0.4–19.1  $\mu\text{M}$ ) were tailored to answer questions about aging and apoptosis and not resting and exercising muscle (<0.05–1.5  $\mu\text{M}$ ).<sup>17–19</sup> Kavanagh et al.<sup>6</sup> reported that skeletal muscle mitochondria in the presence of  $\text{Ca}^{2+}$  have an increase in flux through the substrate oxidation pathway for NAD-linked fuels as well as the phosphorylation pathway regardless of fuel. However, the inhibitor titrations used by Kavanagh et al.<sup>6</sup> make it difficult to discern effects of  $\text{Ca}^{2+}$  on the ETC from those on the substrate dehydrogenases and/or the ATP-producing and transporting enzymes.

The purpose of this study was to determine the role of  $\text{Ca}^{2+}$  in modulating oxidative phosphorylation in isolated porcine skeletal muscle mitochondria. We hypothesized that  $\text{Ca}^{2+}$

Received: November 28, 2012

Revised: February 15, 2013

Published: April 2, 2013



would increase the maximal velocity of oxidative phosphorylation, as seen in other systems,<sup>8,9,15,20</sup> and that this effect would be the result of a distributed activation of reactions within the oxidative phosphorylation network. This was evaluated by establishing the dose–response effect of  $\text{Ca}^{2+}$  on oxidative phosphorylation and performing force–flow analyses of the oxidative phosphorylation network using concurrent measures of the redox states of NADH and the cytochromes, the extramitochondrial free energy of ATP ( $\Delta G_{\text{ATP}}$ ), and mitochondrial membrane potential ( $\Delta\Psi$ ) to estimate the effective conductance of several of the reaction steps of oxidative phosphorylation in the presence and absence of  $\text{Ca}^{2+}$ .

## ■ EXPERIMENTAL PROCEDURES

**Mitochondrial Isolation and Normalization.** All procedures were approved by the National Heart, Lung and Blood Institute Animal Care and Use Committee and performed in accordance with the guidelines described in the Animal Care and Welfare Act (7 USC 2142 § 13). Skeletal muscle mitochondria from the oxidative, porcine vastus intermedius were isolated using a Percoll gradient as described previously.<sup>21</sup> Mitochondria were normalized to the optically determined cytochrome  $a,a_3$  (cyt  $a$ ) content because this assay was very fast, did not require a standard curve, and provided the actual amount of mitochondrial oxidative phosphorylation complex in the sample independent of cytosolic contaminants. The cyt  $a$  content was measured as described previously,<sup>22</sup> typically yielding a final mitochondrial suspension of 20–35 nmol of cyt  $a$ /mL. Purified porcine skeletal muscle mitochondria contain  $\sim 1.0$  nmol of cyt  $a$ /mg of protein.<sup>21</sup>

**Mitochondrial Respiration, NADH, and Membrane Potential.** Mitochondrial oxygen consumption ( $J_o$ ), NADH fluorescence, and membrane potential ( $\Delta\Psi$ ) were measured simultaneously and continuously in a water-jacketed chamber maintained at 37 °C as described previously.<sup>9,23</sup> Experiments were conducted with mitochondria (375 pmol of cyt  $a$ ) in a 1.5 mL final volume of respiration medium (RM) containing 100 mM KCl, 50 mM MOPS, 20 mM glucose, 15 mM NaCl, 10 mM  $\text{MgCl}_2$ , 1 mM EGTA, and 0.2% (w/v) BSA (pH 7.0).  $J_o$  was measured using a Clark electrode and an oxygen solubility of 199 nmol/mL at 37 °C.<sup>24</sup>

The NADH reduction level was calculated relative to the fully oxidized ( $\text{Ca}^{2+}$ -depleted mitochondria, no added substrates, with ADP and  $\text{P}_i$ ) and fully reduced (mitochondria with added substrates and  $\text{Ca}^{2+}$  at anoxia) states.  $\Delta\Psi$  was determined on the basis of the distribution of the lipophilic cation TPP<sup>+</sup> across the inner mitochondrial membrane using a TPP<sup>+</sup> sensitive microelectrode (KWIKTPP, World Precision Instruments). Binding of TPP<sup>+</sup> to mitochondria was accounted for as described previously.<sup>9</sup> With 10 mM  $\text{P}_i$  in RM for all experiments along with sodium in the medium, the contribution of the pH gradient ( $\Delta\text{pH}$ ) to the protonmotive force ( $\Delta\text{pH} + \Delta\Psi$ ) was assumed to be insignificant.<sup>25</sup>

**Experimental Conditions.** For all respiration experiments, mitochondria were incubated in RM at 37 °C in the presence of sodium and in the absence of exogenous substrates or energy phosphates to deplete endogenous  $\text{Ca}^{2+}$  from the mitochondrial matrix.<sup>5,6,9</sup> After the depletion step, 10 mM  $\text{P}_i$  and 0.13 mM ADP were added, followed by glutamate (G, 10 mM) and malate (M, 1 mM) with or without  $\text{Ca}^{2+}$ . Addition of fuel (G + M) initiated a submaximal increase in  $J_o$  followed by a subsequent transition to State 4  $J_o$ . For experiments designed to measure maximal  $J_o$ , State 3 was then elicited with a bolus of 1.3

mM ADP, which resulted in consumption of all the oxygen in the chamber providing the fully reduced state (anoxia). Free  $\text{Ca}^{2+}$  concentrations were determined using the calculator programs of Fabiato and Fabiato<sup>26</sup> translated to Labview VIs (National Instruments Corp., Austin, TX) by Reitz and Pollack.<sup>27</sup>

Steady-state, intermediate  $J_o$  was attained using a progressive creatine kinase (CK) energetic clamp<sup>28</sup> that we have recently modified.<sup>29</sup> Briefly, by utilizing a large total creatine pool, excess CK, a known ATP concentration, and the CK equilibrium constant ( $K_{\text{CK}}$ , 150),<sup>30</sup> the extramitochondrial ATP/ADP ratio and, thus, free energy of ATP hydrolysis ( $\Delta G_{\text{ATP}_e}$ ) can be calculated from the added phosphocreatine (PCr)/creatine (Cr) ratio:

$$\Delta G_{\text{ATP}_e} = \Delta G_{\text{ATP}}^\circ - 2.3RT \log\left[\frac{[\text{PCr}]K_{\text{CK}}}{([\text{Cr}][\text{P}_i])}\right] \quad (1)$$

where  $\Delta G_{\text{ATP}}^\circ$  is the standard  $\Delta G_{\text{ATP}}$  (−7.592 kcal/mol),  $R$  is the gas constant (1.987 cal K<sup>−1</sup> mol<sup>−1</sup>), and  $T$  is the temperature (310 K). Mitochondria oxidizing G+M at State 4 were given 2.5 mM PCr, 5 mM Cr, 5 mM ATP, and 75 units/mL CK, resulting in a  $J_o$  of  $\sim 2/3$  of State 3. Subsequent additions of PCr (to 3.75, 5, 7.5, and 10 mM) were made to slow  $J_o$  to  $\sim 1/3$  of State 3.

Additional experiments with pyruvate similar to those of Messer et al.<sup>28</sup> were conducted. Briefly, mitochondria in the presence of a saturating level of M were exposed to the CK clamp as described above with a PCr/Cr ratio of 0.25. Pyruvate was then titrated in stepwise at 10, 25, 50, 100, and 500  $\mu\text{M}$  to increase the level of respiration. The novel aspect of this experiment was that upon reaching a steady state with 500  $\mu\text{M}$  pyruvate, stepwise additions of PCr were then made to slow  $J_o$ . Thus, in a single experiment,  $J_o$  was changed by both “push” (pyruvate titration) and “pull” (CK clamp) mechanisms.

**Mitochondrial Optical Absorption.** A system was developed from our earlier work with an integrating sphere to minimize the effects of light scattering on the visible spectrum of mitochondrial suspensions.<sup>23</sup> Our current implementation permits studies of well-mixed samples at physiological temperatures with a complete linear regression analysis of the chromophores of oxidative phosphorylation.<sup>31</sup> Briefly, a 6 in. integrating sphere (model RTC-060-SF, LabSphere, Inc., North Sutton, NH) was used with a custom-designed, 1.2 cm diameter, cylindrical, water-jacketed, center-mounted chamber to hold the mitochondrial suspension. The volume used in this chamber was 2 mL. The sample was uncapped, and oxygen consumption measurements in the chamber were not attempted because of the optical interference of electrodes. All oxygen consumption data were collected in parallel in a dedicated polarography chamber at the same temperature. All experiments were conducted at 37 °C. White light (model CS-16-500, Jobin-Yvon, Inc., Spex Forensics Division, Edison, NJ) was impinged on the sample, and the absorbed light was collected via a fiber optic using the sampling port on the sphere. Rapid-scanning optical spectra (one spectrum per 100 ms) were collected using a photodiode array (model QE-65000, Ocean Optics, Inc.) from  $\sim 300$  to 800 nm. Analysis was conducted on the  $\beta$  and  $\alpha$  bands of the cytochromes from the 466–630 nm region because this provided the best discrimination of the absorbance bands.<sup>31</sup>

Data analysis was performed by completely fitting the absorbance difference spectra to seven reference difference spectra for FAD, cytochrome  $b_H$ , cytochrome  $b_L$ , cytochrome

$c_1$ , cytochrome  $c$ , cytochrome  $a_3$  peroxy form ( $a_{607}$ ), cytochrome  $a_3$  ferryl form ( $a_{580}$ ), and a simple linear term for baseline corrections as previously described using linear regression fitting.<sup>31</sup> The fully oxidized state was taken as mitochondria in the absence of carbon substrates and the addition of ADP and  $P_i$ . The fully reduced state for FAD and cytochromes  $b_H$ ,  $c_1$ ,  $c$ , and  $a_{607}$  was obtained by adding a small amount of sodium hydrosulfite at the end of the experiment. Cytochromes  $b_L$  and  $a_{580}$  were most reduced under State 4 conditions; thus, State 4 was considered to be full reduction for these two species. The cytochrome  $a_{580}$  reduction level was then normalized to total cyt  $a$  content assuming a  $1/2 a_{580}/a_{607}$  extinction coefficient ratio.<sup>32,33</sup>

**Driving Forces and Pathway Conductances.** In this study, the force-flow behavior for different regions of the oxidative phosphorylation network was used to estimate the effective conductance (or resistance) of each region during active oxidative phosphorylation. This is in contrast to studies of isolated protein complexes in native gels that alter the pathway using inhibitor titrations in which oxidative phosphorylation is not proceeding under normal conditions. To accomplish this task, the oxidation/reduction (redox) potentials ( $E_h$ ) of the products and reactants of a reaction segment, as well as  $\Delta\Psi$  when appropriate, must be determined for the driving force, while  $J_o$  provides the flux for all of the elements. Mitochondrial complex  $E_h$  for redox pairs was calculated as

$$E_h = E_m + 2.3(RT/nF) \times \log([\text{oxidized}]/[\text{reduced}]) \quad (2)$$

where  $E_m$  is the midpoint potential (−320 mV for NAD/NADH, 230 mV for cyt  $c_1$ , 270 mV for cyt  $c$ , 280 mV for cyt  $a_{607}$ , and 820 mV for  $O_2/H_2O$ <sup>34–37</sup>),  $n$  is the number of electrons to be transferred, and  $F$  is the Faraday constant (23.062 cal  $mV^{-1}$   $mol^{-1}$ ). Free energies ( $\Delta G$ ) were calculated assuming that a single NADH donates two electrons ( $n$ ) to the ETC, resulting in 10 protons being pumped ( $m$ ) that, in turn, yields 2.7 ATP molecules ( $p$ ):

$$\Delta G_{\text{redox}} = -nF(\Delta E_h + z\Delta\Psi) \quad (3)$$

$$\Delta G_{\Delta\Psi} = -mF\Delta\Psi \quad (4)$$

$$\Delta G_{\text{ATP}} = p\Delta G_{\text{ATP}e} \quad (5)$$

where eq 3 is used for the free energy driving electron transfer with  $\Delta E_h$  as the redox potential difference and  $z$  as the relative distance across the mitochondrial inner membrane relative to the matrix side between two redox pairs, eq 4 is used for the free energy associated with pumping protons across the mitochondrial inner membrane, and eq 5 is used for the stoichiometric free energy of ATP hydrolysis. For electron transfer steps within the ETC,  $m$  was varied according to the number of protons moved across the mitochondrial inner membrane between the respective electron donors and acceptors, and  $z$  was assumed to be 1, 0, 0, and −1 for electron transfer between NADH and cyt  $c_1$ , cyt  $c_1$  and cyt  $c$ , cyt  $c$  and cyt  $a_{607}$ , and cyt  $a_{607}$  and  $O_2$ , respectively, yielding a value of 0 for electron flow down the entire ETC.

Flux down an oxidative phosphorylation pathway was assumed to vary according to the thermodynamic driving forces acting on it using classical irreversible thermodynamic approaches:<sup>38,39</sup>

$$J = L(\Delta G_1 - \Delta G_2) \quad (6)$$

where  $J$  is the flux down the pathway,  $L$  is the phenomenological transport coefficient of the reaction, and  $\Delta G_1$  and  $\Delta G_2$  are the driving forces acting on the front and back ends of the pathway, respectively. For the purposes of this discussion, we will refer to the transport coefficient,  $L$ , as a “conductance” because many of the reactions we are evaluating involve the displacement of charged species. Simultaneous measurement of oxygen flux ( $J_o$ ) and the thermodynamic driving forces for oxidative phosphorylation ( $\Delta G_{\text{redox}}$ ,  $\Delta G_{\Delta\Psi}$ , and  $\Delta G_{\text{ATP}}$ ) thus allows for the calculation of the conductances of the ETC ( $\Delta G_{\text{redox}} - \Delta G_{\Delta\Psi}$ ), ATP synthesis/transport ( $\Delta G_{\Delta\Psi} - \Delta G_{\text{ATP}}$ ), and complete oxidative phosphorylation pathways ( $\Delta G_{\text{redox}} - \Delta G_{\text{ATP}}$ ). With a saturating level of oxidative substrates, we considered the free energy associated with the added fuel to be constant. As such, we were also able to calculate the conductance of the fuel transport/dehydrogenase pathway ( $\Delta G_{\text{fuel}} - \Delta G_{\text{NADH}}$ ) and of the complete mitochondrial energy conversion process ( $\Delta G_{\text{fuel}} - \Delta G_{\text{ATP}}$ ) using the  $\Delta G_{\text{NADH}}$  and  $\Delta G_{\text{ATP}}$  relationships with  $J_o$ , respectively.

**Stoichiometries.** The ratios of protons pumped across the inner membrane per electron passed ( $H^+/e^-$ ) were measured using the force ratio.<sup>40–42</sup> Briefly, the ratio of the respective thermodynamic forces was plotted against  $J_o$ , and from the resultant linear relationship, the force ratio at zero flux ( $x$ -intercept) could be extrapolated. Under equilibrium conditions, plugging eqs 3 and 4 into eq 5 and rearranging yield the following:

$$m/n = \Delta E_h/\Delta\Psi + z \quad (7)$$

where  $m/n$  is the  $H^+/e^-$  ratio. The experimentally determined stoichiometries were then compared to those used in the  $\Delta G$  calculations to provide a measure of validity.

**Statistical Analysis.** For the  $Ca^{2+}$  titration experiments, significant differences were assessed using a repeated measures analysis of variance with a Tukey–Kramer multiple-comparison post hoc test. Differences in slopes between  $Ca^{2+}$  and no  $Ca^{2+}$  conditions were assessed using a two-tailed, paired Student’s  $t$  test. A  $p$  value of 0.05 was used to determine statistical significance.

## RESULTS

**Maximal Respiration.** State 3  $J_o$  as well as State 3 and 4 NADH levels increased with an increasing  $Ca^{2+}$  concentration up to 840 nM, beyond which a plateau occurred (Figure 1). The initial increase in State 3 with  $Ca^{2+}$  was linear with a slope of 0.33 nmol of  $O_2$   $min^{-1}$  (nmol of cyt  $a$ )<sup>−1</sup> (nM  $Ca^{2+}$ )<sup>−1</sup>. The optimal  $Ca^{2+}$  dose (840 nM) for respiration resulted in a 1.8-fold increase in State 3  $J_o$  [ $405.9 \pm 12.6$  nmol of  $O_2$   $min^{-1}$  (nmol of cyt  $a$ )<sup>−1</sup>] compared to that with no  $Ca^{2+}$  [ $226.8 \pm 17.5$  nmol of  $O_2$   $min^{-1}$  (nmol of cyt  $a$ )<sup>−1</sup>]. Surprisingly, the optimal  $Ca^{2+}$  dose had no effect on  $\Delta\Psi$  at State 3 and State 4 despite the large increase in NADH and  $J_o$ . This result implies that the effects of  $Ca^{2+}$  cannot be caused by alterations in  $\Delta\Psi$  alone as other processes must be affected.

The mitochondrial isolation process typically results in mitochondria with high endogenous levels of  $Ca^{2+}$ .<sup>43,44</sup> Depletion of endogenous calcium for these experiments was achieved through a 6 min mitochondrial incubation period at 37 °C without added substrates in the presence of 15 mM sodium (to stimulate  $Na^+/Ca^{2+}$  exchange), which we have previously shown to remove nearly all  $Ca^{2+}$  from the mitochondrial matrix.<sup>45</sup> This incubation step resulted in a State 3  $J_o$  that was 49% of the rate without incubation or NaCl



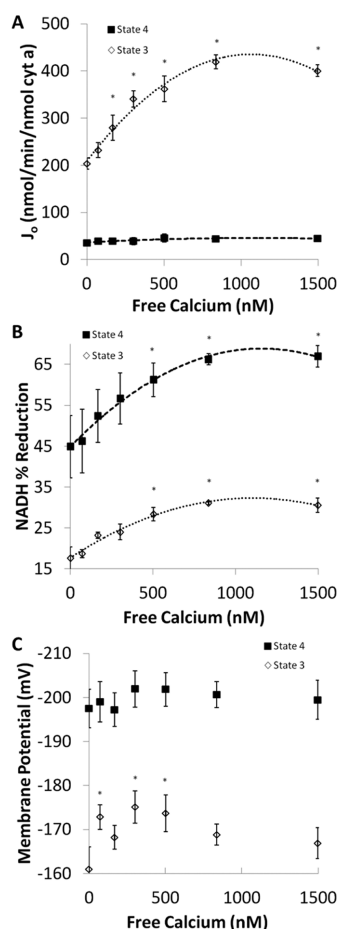


**Figure 1.** Calcium titration. (A) State 3 and 4  $J_o$  at added free calcium concentrations from 0 to 1500 nM. (B) State 3 and 4 NADH at added free calcium concentrations from 0 to 1500 nM. (C) State 3 and 4  $\Delta\Psi$  at added free calcium concentrations from 0 to 1500 nM. For all panels: (■) State 4 and (◇) State 3. Error bars signify the standard error. Asterisks denote a significant difference from the no calcium condition.  $n = 4$ .

(Table 1). Addition of  $\text{Ca}^{2+}$  after the incubation period resulted in a State 3  $J_o$  that was 88% of the rate without incubation, which is consistent with the notion that the effects of the incubation period are primarily due to a depletion of  $\text{Ca}^{2+}$ .

**Steady-State, Intermediate Respiration.** A representative trace of a CK clamp experiment is shown in Figure 2, and the resultant linear relationship between  $\Delta G_{\text{ATP}_e}$  and  $J_o$  is presented in Figure 3A.<sup>3,46,47</sup> A roughly 2-fold increase in the level of respiration was observed with calcium at each clamped  $\Delta G_{\text{ATP}_e}$  value (Figure 3A). Therefore, the ability to produce ATP with fixed substrate and product concentrations was enhanced by  $\text{Ca}^{2+}$ . This result implied that the  $V_{\text{max}}$  of the

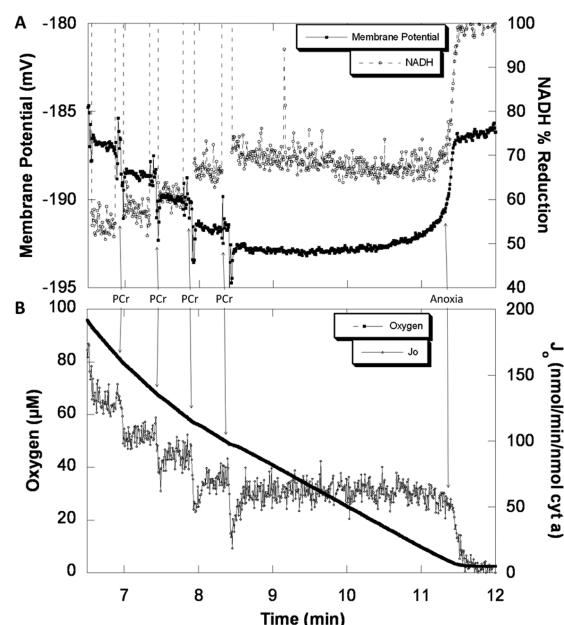


**Figure 2.** Representative CK energetic clamp experiment. (A)  $\Delta\Psi$  and NADH during stepwise PCr additions and under anoxic conditions. (B)  $J_o$  and  $[\text{O}_2]$  during stepwise PCr additions and at anoxic conditions.

mitochondria for producing ATP was increased by  $\text{Ca}^{2+}$ . To confirm this notion, these data were reformulated to extract the affinity of oxidative phosphorylation for ADP. In Figure 3B, the dose–response curve of ADP concentration versus  $J_o$  reveals typical saturating kinetics. The Eadie–Hofstee plot in Figure 3C demonstrates that the increase in  $J_o$  with  $\text{Ca}^{2+}$  was not due to a change in ADP affinity,  $\sim 43 \mu\text{M}$ , but rather to a doubling of the  $V_{\text{max}}$  from  $\sim 200$  to  $\sim 425 \text{ nmol min}^{-1} (\text{nmol of cyt a})^{-1}$ , consistent with the data presented in Figure 1. It is important to note that combining the increase in  $V_{\text{max}}$  due to  $\text{Ca}^{2+}$  with the change in ADP from resting muscle ( $\sim 5 \mu\text{M}$ ) to that during modest concentric exercise ( $\sim 25 \mu\text{M}$ ) in humans<sup>48</sup> can explain an  $\sim 7$ -fold increase in respiration rate. These physiological points are highlighted in Figure 3B, and the combined effects of  $\text{Ca}^{2+}$  and ADP are further developed in the Discussion.

The remaining studies focused on isolating the elements within oxidative phosphorylation responsible for the increase in  $V_{\text{max}}$  by  $\text{Ca}^{2+}$ . To evaluate the contribution of different steps in the oxidative phosphorylation network, the phenomenological conductance was determined for each step for which the net driving forces could be measured. The primary potential energy for oxidative phosphorylation, especially with the substrates we utilized, is the free energy in NADH that is then converted into  $\Delta\Psi$ . The force–flow relationships for these parameters are presented in Figure 4, where the convention of the force, net

**Table 1.** Oxygen Consumption, NADH Level Reduction, and Membrane Potential at Maximal and Resting Respiration<sup>a</sup>

incubation conditions	$J_o^b$		NADH <sup>c</sup>		$\Delta\Psi^d$	
	State 4	State 3	State 4	State 3	State 4	State 3
no calcium ( $n = 9$ )	$31.0 \pm 3.2$	$226.8 \pm 17.5^f$	$59.9 \pm 5.1$	$17.8 \pm 1.3$	$-202.1 \pm 2.6$	$-171.5 \pm 4.1$
calcium ( $n = 9$ )	$39.8 \pm 3.1^e$	$405.9 \pm 12.6^{ef}$	$72.4 \pm 2.9^e$	$30.0 \pm 1.3^e$	$-203.1 \pm 1.5$	$-174.9 \pm 2.2$
no NaCl, no depletion, no calcium ( $n = 12$ )	$29.3 \pm 3.7$	$463.2 \pm 19.0$				

<sup>a</sup>Skeletal muscle mitochondria oxidizing 10 mM glutamate and 1 mM malate. Values are means  $\pm$  the standard error. <sup>b</sup> $J_o$  values are in units of nanomoles of  $\text{O}_2$  per minute per nanomole of cyt a. <sup>c</sup>NADH values are in units of percent reduced. <sup>d</sup> $\Delta\Psi$  values are in units of millivolts. <sup>e</sup>Denotes significant difference between calcium and no calcium. <sup>f</sup>Denotes significant difference from the no depletion condition.

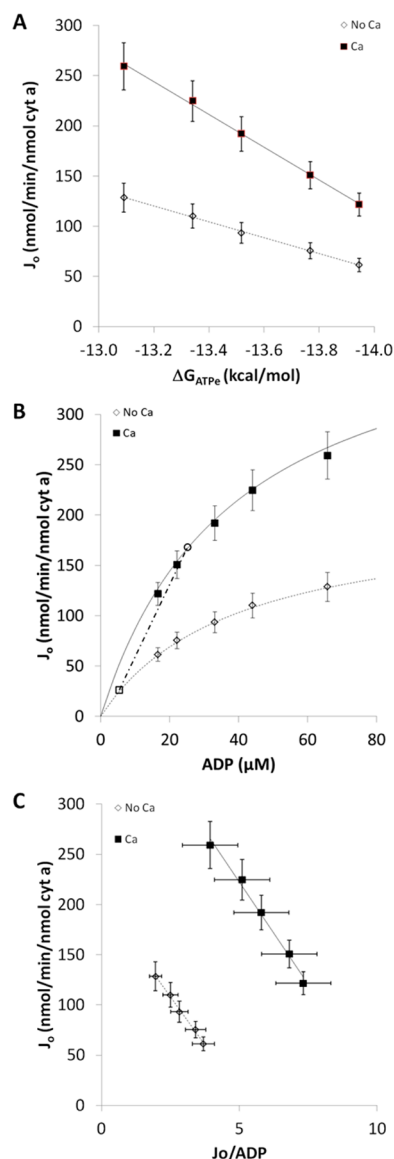


**Figure 3.** Kinetic effect of calcium on oxidative phosphorylation intermediate respiration. (A) Relationship between  $\Delta G_{ATPe}$  and  $J_o$  with and without calcium. (B) Michaelis-Menten relationship between  $J_o$  and ADP with and without calcium. The empty square and empty circle signify the ADP values reported for human skeletal muscle at rest and during moderate exercise, respectively. (C) Eadie-Hofstee plot for the relationship between  $J_o$  and ADP, where  $y = -(K_{mADP})x + V_{max}$ . For all panels: (■) calcium and (◇) no calcium. Error bars signify the standard error.  $n = 12$ . Slopes, regression analyses, and the resultant  $p$  values for panels A and C are listed in Table 2 under  $\Delta G_{ATPe}$  and  $K_{mADP}$ , respectively.

NADH or  $\Delta\Psi$ , is plotted on the X-axis and flow,  $J_o$ , is plotted on the Y-axis. The force-flow relationships for NADH and  $\Delta\Psi$  were linear for both the control and  $Ca^{2+}$  conditions.  $Ca^{2+}$  increased the force-flow slopes by  $\sim 0.7$ - and  $2.1$ -fold for NADH and  $\Delta\Psi$ , respectively (Table 2). These data are consistent with previous observations in porcine heart mitochondria.<sup>9</sup> The relationships in Figure 4 provide only a measure of the balance between production and utilization of the respective free energies, NADH or the resulting  $\Delta\Psi$ ; thus, many different parameters could contribute to the  $Ca^{2+}$ -induced changes in total velocity and slope, including dehydrogenase activity, ADP kinetics on  $F_1F_0$ ATPase velocity, or any

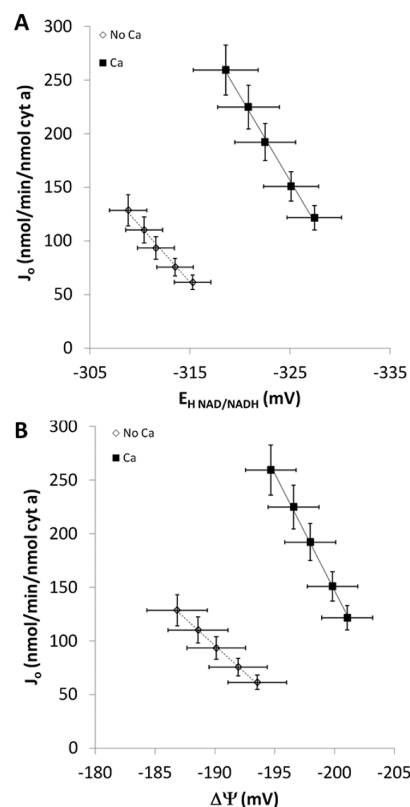


**Figure 4.** Effect of calcium on oxidative phosphorylation energetic driving forces and  $J_o$  during intermediate respiration. (A) Relationship between NADH and  $J_o$  with and without calcium. (B) Relationship between  $\Delta\Psi$  and  $J_o$  with and without calcium. For all panels: (■) calcium and (◇) no calcium. Error bars signify the standard error.  $n = 12$ . Slopes, regression analyses, and the resultant  $p$  values are listed in Table 2.

alterations within the ETC. Thus, to determine the specific locations of  $Ca^{2+}$  sensitivity, we used the free energy differences measured across various spans of the mitochondrial energy conversion pathway along with  $J_o$  to determine the conductance or, reciprocally, the resistance to energy flow of each span. Figure 5 depicts the thermodynamic driving forces measured and the energy conversion steps for which conductances were calculated.

The conductance of the entire oxidative phosphorylation cascade,  $L_{oxphos}$ , was determined by plotting  $J_o$  versus  $(\Delta G_{NADH} - \Delta G_{O_2}) - \Delta G_{ATP}$ , the potential energy across the oxidative phosphorylation process. It is important to note that because the  $\Delta G_{NADH}$  is included in this calculation, the effects of dehydrogenase activation are eliminated from this force-flow relationship, which is presented in Figure 6A. The overall  $L_{oxphos}$  increased 2.0-fold in the presence of  $Ca^{2+}$ . These data are consistent with the notion that the ability of oxidative phosphorylation to generate ATP at a given free energy is improved in the presence of  $Ca^{2+}$ .

It has been previously established that the maximal activity of Complex V is increased by  $Ca^{2+}$ .<sup>9</sup> We confirmed that the ATP synthesis mechanism,  $L_{ATPase}$ , which includes both Complex V and the adenylate nucleotide translocase (ANT), was activated by  $Ca^{2+}$  by plotting  $J_o$  versus  $\Delta\Psi - \Delta G_{ATP}$  in Figure 6B. The calculated  $L_{ATPase}$  increased by a factor of 2.4 in the presence of  $Ca^{2+}$  (Table 2), which is consistent with previous results in the porcine heart<sup>9</sup> and recent biochemical analysis.<sup>49</sup>

Table 2. Mean Values for Force–Flow Relationships in Figures 3, 4, 6, 8, and 9<sup>a</sup>

	slope		$r^2$		$p$ value <sup>c</sup>
	no calcium	calcium	no calcium	calcium	
NADH (mV)	12.2 ± 2.6	20.5 ± 4.0 <sup>b</sup>	0.981 ± 0.004	0.960 ± 0.013	0.010
cyt $b_H$ (% reduced)	16.0 ± 2.9	−75.6 ± 40.5	0.518 ± 0.192	0.558 ± 0.200	0.108
cyt $b_L$ (% reduced)	−3.0 ± 0.2	−8.2 ± 1.1 <sup>b</sup>	0.961 ± 0.006	0.937 ± 0.018	0.021
cyt $c_1$ (% reduced)	−15.9 ± 27.7	−31.8 ± 21.2	0.527 ± 0.168	0.268 ± 0.139	0.587
cyt $c$ (% reduced)	−53.6 ± 10.5	−16.1 ± 53.0	0.568 ± 0.119	0.498 ± 0.109	0.518
cyt $a_{607}$ (% of total cyt $a$ )	67.9 ± 17.9	87.8 ± 32.5	0.937 ± 0.022	0.893 ± 0.053	0.678
cyt $a_{580}$ (% of total cyt $a$ )	4.6 ± 13.1	95.2 ± 24.4	0.528 ± 0.235	0.799 ± 0.055	0.073
$\Delta\Psi$ (mV)	10.3 ± 1.4	22.1 ± 2.5 <sup>b</sup>	0.989 ± 0.004	0.989 ± 0.002	0.000
$\Delta G_{ATP_e}$ (kcal/mol)	80.0 ± 11.3	163.2 ± 17.9 <sup>b</sup>	0.991 ± 0.002	0.990 ± 0.002	0.000
$K_{mADP}$ ( $\mu$ M)	42.3 ± 6.6	44.4 ± 6.3	0.963 ± 0.010	0.942 ± 0.023	0.687
$L_{fuel/DH}$	−263.5 ± 57.3	−445.3 ± 87.1 <sup>b</sup>	0.981 ± 0.004	0.960 ± 0.013	0.010
$L_{CI+III}$	−101.9 ± 20.9	−224.7 ± 17.0 <sup>b</sup>	0.992 ± 0.001	0.927 ± 0.043	0.012
$L_{c1c}$	−91.0 ± 116.2	269.3 ± 191.7	0.228 ± 0.078	0.122 ± 0.081	0.266
$L_{CIVa}$	226.4 ± 56.0	543.7 ± 46.3 <sup>b</sup>	0.935 ± 0.016	0.856 ± 0.064	0.043
$L_{CIVb}$	−55.8 ± 13.5	−123.8 ± 25.9 <sup>b</sup>	0.989 ± 0.004	0.970 ± 0.021	0.036
$L_{ETC}$	−39.3 ± 5.6	−96.0 ± 11.1 <sup>b</sup>	0.988 ± 0.005	0.980 ± 0.008	0.000
$L_{ATPase}$	−79.5 ± 37.1	−192.5 ± 33.7 <sup>b</sup>	0.889 ± 0.035	0.969 ± 0.010	0.005
$L_{oxphos}$	−29.8 ± 4.8	−60.9 ± 7.9 <sup>b</sup>	0.989 ± 0.003	0.990 ± 0.003	0.000
$L_{mito}$	−29.6 ± 4.2	−60.4 ± 6.6 <sup>b</sup>	0.991 ± 0.002	0.990 ± 0.002	0.000

<sup>a</sup>Values are means ± the standard error. <sup>b</sup>Denotes significantly different from the no calcium condition. <sup>c</sup>The  $p$  value compares no calcium and calcium slopes.

To eliminate  $L_{ATPase}$  from the conductance calculation, we determined the conductance of the electron transport chain,  $L_{ETC}$ , using  $(\Delta G_{NADH} - \Delta G_{O_2}) - \Delta G_{\Delta\Psi}$  to take into account only the free energy driving the ejection of charge and not ATP synthesis. As seen in Figure 6C,  $L_{ETC}$  was increased 2.4-fold in the presence of  $Ca^{2+}$ . These data suggest that  $Ca^{2+}$  is activating the ETC in a manner independent of effects on Complex V or dehydrogenases.

Using the cytochrome spectra as shown in Figure 7, we could isolate different regions of the ETC to examine whether  $Ca^{2+}$  was altering the reaction kinetics. Force–flow relationships for cytochromes  $b_H$ ,  $b_L$ ,  $c_1$ ,  $c$ , and  $a$  peroxy ( $a_{607}$ ) and ferryl ( $a_{580}$ ) with and without  $Ca^{2+}$  are shown in Figure 8A–F, respectively.  $Ca^{2+}$  caused a greater reduction of all cytochromes with the exception of cyt  $b_L$ . However, the slope of the relationship between  $b_L$  and  $J_o$  was increased 2.7-fold by  $Ca^{2+}$ . The thermodynamic relationships and the chromophores detected provided the differential driving forces for the flux between NADH and cyt  $c_1$  (for calculating  $L_{CI+III}$ ), cyt  $c_1$  and cyt  $c$  (for calculating  $L_{c1c}$ ), cyt  $c$  and cyt  $a_{607}$  (for calculating  $L_{CIVa}$ ), and cyt  $a_{607}$  and oxygen (for calculating  $L_{CIVb}$ ). The use of cyt  $b$  redox forms for calculating a driving force was complicated by the Q cycle; thus, Complex III was lumped with Complex I in  $L_{CI+III}$ .

The calculations of the conductance of the different portions of the ETC are presented in Figure 9A–D. All of the complexes of the ETC were activated by  $Ca^{2+}$ , with  $L_{CI+III}$  increasing 2.2-fold (Figure 9A),  $L_{CIVa}$  increasing 2.4-fold (Figure 9C), and the terminal reaction with oxygen,  $L_{CIVb}$ , increasing 2.2-fold (Figure 9D). These calculations suggest that  $Ca^{2+}$  had a ubiquitous effect on the activity of the electron transport system consistent with activation within Complex I/Complex III and the interactions within Complex IV.

**Resistance to Mitochondrial Energy Conversion.** By considering mitochondrial energy conversion as flux across a series of resistors (see Figure 5), we were able to calculate the contribution of each span of the energy conversion process to

the total resistance to energetic flux. These results are listed in Table 3 where, in the absence of  $Ca^{2+}$ , Complex IV was determined to provide the most resistance to flux followed by Complex I+III, ATP production/transport, and fuel transport/dehydrogenases. Note that the resistance from cyt  $c$  to cyt  $a_{607}$  was considered negligible as  $\Delta G_{cyt\ c-cyt\ a_{607}}$  became more positive as  $J_o$  increased (Figure 9C), suggesting this reaction provides no flux control. Resistance between cyt  $c_1$  and cyt  $c$  was also omitted from this analysis as there was little change in this free energy difference with neither a positive or negative relationship to flux (Table 2). Despite increasing conductances throughout the entire mitochondrial energy conversion pathway, addition of  $Ca^{2+}$  caused a shift in the relative contribution to resistance away from the ETC (both Complex I+III and Complex IV).

**Stoichiometries.** Measuring the force ratios for the spans of the ETC provided validation for the stoichiometries chosen for making the free energy and, thus, conductance calculations described above. The ~10% difference between measured and used values in Table 4 suggests that the numbers of electrons ( $n$ ) and protons ( $m$ ) were correctly assigned when using eqs 3 and 4 for the relationships depicted in Figures 6 and 9 and Tables 2 and 3.

## DISCUSSION

**Steady-State Kinetic Analysis.** Skeletal muscle free  $Ca^{2+}$  levels are typically less than 50 nM at rest and, at the onset of exercise, can transiently increase to 0.5–1.5  $\mu$ M, depending on both intensity and modality.<sup>17,18,50</sup> Using the reported skeletal muscle values as a guide,  $Ca^{2+}$ -depleted skeletal muscle mitochondria were incubated at  $\leq 1.5\ \mu$ M to determine the steady-state kinetic relationship between  $Ca^{2+}$  and State 3 and State 4  $J_o$ , NADH, and  $\Delta\Psi$ , as well as the optimal  $Ca^{2+}$  dose for stimulating oxidative phosphorylation (Figure 1). The kinetic relationship to  $Ca^{2+}$  was similar between  $J_o$  and NADH, with both being maximally stimulated at 840 nM  $Ca^{2+}$ . Thus, the

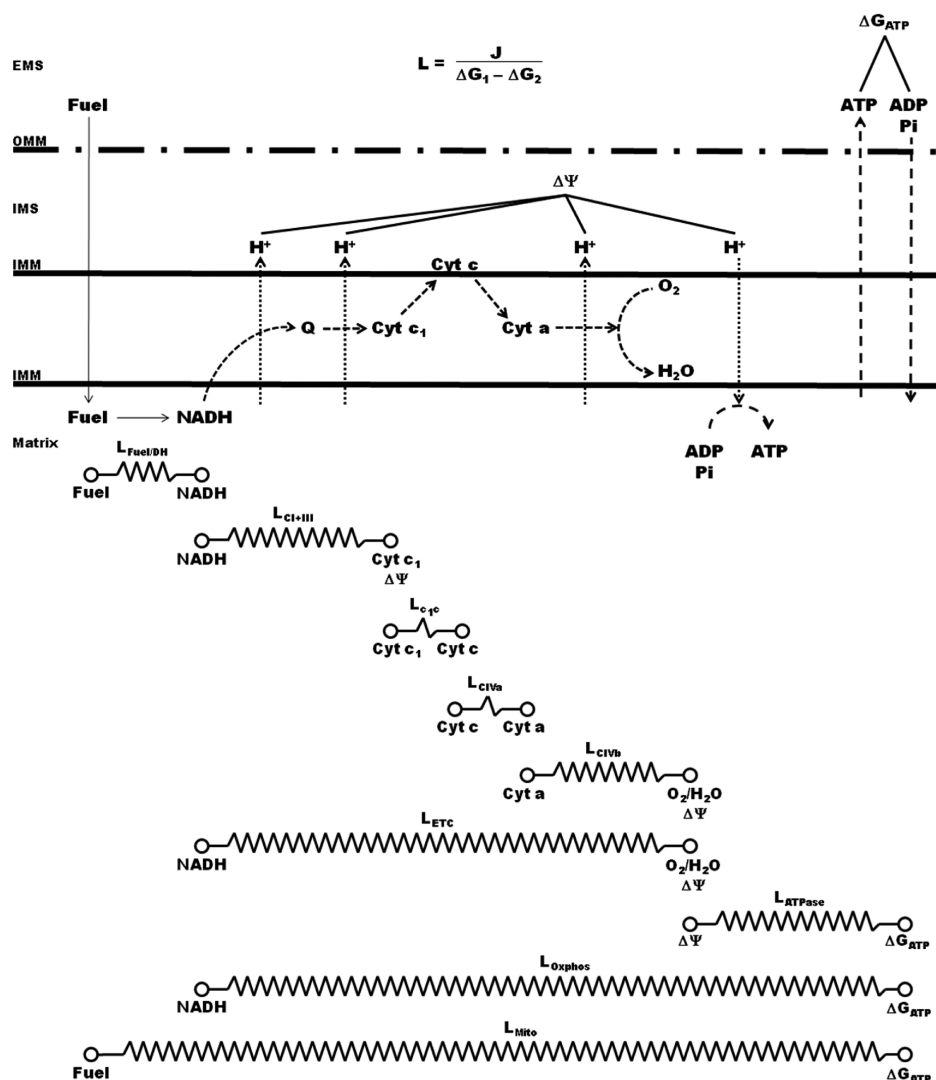


**Figure 5.** Simple model of the mitochondrial energy conversion cascade. The path of energy flow is depicted in the top half, while the measured energetic driving forces and how they relate to the calculation of conductances or resistances are depicted in the bottom half.

optimal  $\text{Ca}^{2+}$  dose for oxidative phosphorylation in isolated mitochondria is similar to that in exercising muscle, and as a result, the  $\text{Ca}^{2+}$  levels used in this study may offer some insight into the  $\text{Ca}^{2+}$  activation of mitochondria in the transition from rest to exercise. It should be noted that the temporal kinetics of exposure of the mitochondria to  $\text{Ca}^{2+}$  in these studies with constant step changes is much different than the transient nature of cytosolic  $\text{Ca}^{2+}$ , *in vivo*. Thus, these steady-state, *in vitro* kinetics can only be estimates of the *in vivo* conditions. Further kinetic analysis revealed that the increase in State 3  $J_o$  with  $\text{Ca}^{2+}$  was the result of an increase in the apparent  $V_{\max}$  of oxidative phosphorylation and not the result of changes in ADP affinity (Figure 3C) as previously shown by Scaduto's group in heart mitochondria.<sup>8</sup> However, because we used saturating concentrations of carbon substrates and a limited number of substrates, we cannot reach conclusions regarding carbon substrate affinity changes to  $\text{Ca}^{2+}$ . The remainder of the study focuses on unraveling the mechanism of the  $\text{Ca}^{2+}$ -induced  $V_{\max}$  increase in skeletal muscle mitochondria under these conditions.

**Force–Flow Analysis.** Simultaneous measurement of  $J_o$ ,  $\Delta\Psi$ , and the NADH and cytochrome redox states at several different respiration rates allows for a novel evaluation of the

impact of  $\text{Ca}^{2+}$  on metabolic flux and thermodynamic driving forces. The CK clamp provides mitochondria with extra-mitochondrial  $\Delta G_{\text{ATP}}$  and  $[\text{ADP}]_f$  values similar to those observed in human skeletal muscle *in vivo*.<sup>48,51,52</sup> Thus, we were able to examine the effects of  $\text{Ca}^{2+}$  in an environment that may more closely approximate *in vivo* conditions compared to experiments using inhibitors and/or excess ADP.

Initial force–flow analyses examined the effect of  $\text{Ca}^{2+}$  on the conductance of the overall mitochondrial energy conversion cascade ( $L_{\text{mito}}$ ) by measuring the slope of the relationship between flux ( $J_o$ ) and the difference between the forward ( $\Delta G_{\text{fuel}}$ ) and reverse ( $\Delta G_{\text{ATP}}$ ) driving forces (eq 6 and Figure 5). Because  $\Delta G_{\text{fuel}}$  is assumed to be constant at the high substrate concentrations used,  $\Delta G_{\text{fuel}} - \Delta G_{\text{ATP}}$  is reduced to  $\Delta G_{\text{ATP}}$  for this analysis. Using this simplification, the 2.0-fold increase in the  $J_o/\Delta G_{\text{ATP}}$  slope shown in Figure 3A represents a 2.0-fold increase in  $L_{\text{mito}}$ , nearly identical to the  $\text{Ca}^{2+}$ -induced increase in State 3  $J_o$  discussed above. However,  $L_{\text{mito}}$ , much like State 3  $J_o$ , gives only a global view of the effect of  $\text{Ca}^{2+}$  on oxidative phosphorylation with no information about the specific sites that are affected. To remove the influence of fuel transportation and substrate dehydrogenases on  $L_{\text{mito}}$ , we used the NADH redox status along with  $\Delta G_{\text{ATP}}$  to calculate



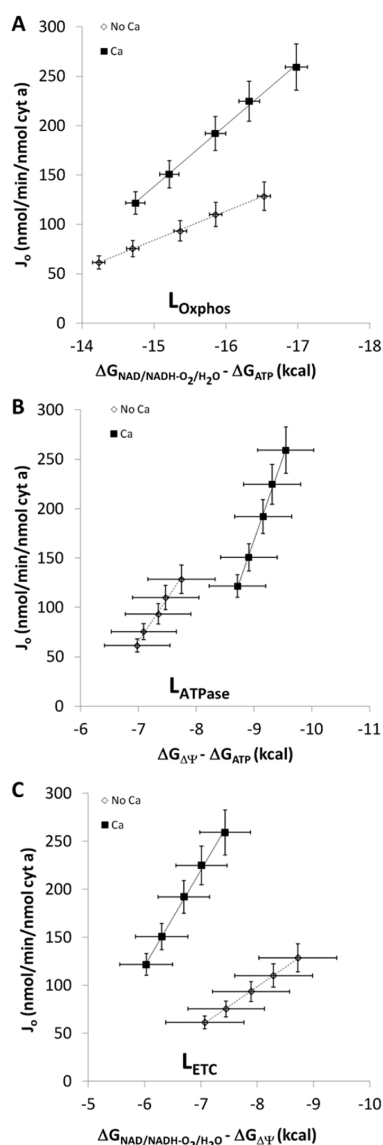


**Figure 6.** Effect of calcium on mitochondrial conductances. (A) Relationship between  $J_o$  and the free energy difference between NADH and  $\Delta G_{\text{ATP}}$  with and without calcium. (B) Relationship between  $J_o$  and the free energy difference between  $\Delta\Psi$  and  $\Delta G_{\text{ATP}}$  with and without calcium. (C) Relationship between  $J_o$  and the free energy difference between NADH and  $\Delta\Psi$  with and without calcium. For all panels: (■) calcium and (◇) no calcium. Error bars signify the standard error.  $n = 12$ . Slopes, regression analyses, and the resultant  $p$  values for panels A–C are listed in Table 2 under  $L_{\text{Oxphos}}$ ,  $L_{\text{ATPase}}$ , and  $L_{\text{ETC}}$  respectively.

$L_{\text{Oxphos}}$ , or the conductance of the oxidative phosphorylation reactions. Just as with  $L_{\text{mito}}$ ,  $\text{Ca}^{2+}$  caused a 2.0-fold increase in  $L_{\text{Oxphos}}$  (Figure 6A). Thus, oxidative phosphorylation was activated by  $\text{Ca}^{2+}$  in a manner independent of the well-known effects of  $\text{Ca}^{2+}$  on dehydrogenases and substrate transport.<sup>53</sup> We then split  $L_{\text{Oxphos}}$  into two separate elements, the combination of Complex V and ANT (ATP production/transport,  $L_{\text{ATPase}}$ ) and the ETC ( $L_{\text{ETC}}$ ), by using the measured intermediate,  $\Delta\Psi$ .  $L_{\text{ATPase}}$  was increased 2.4-fold by  $\text{Ca}^{2+}$  (Figure 6B), which is similar to previous reports demonstrating that  $\text{Ca}^{2+}$  activates cardiac Complex V<sup>9,49</sup> and in skeletal muscle where  $\text{Ca}^{2+}$  activated the phosphorylation subsystem.<sup>6</sup>

The conductance of the ETC,  $L_{\text{ETC}}$ , was also increased 2.4-fold by  $\text{Ca}^{2+}$  (Figure 6C). Because a pathway with greater conductance necessitates weaker driving forces to achieve a given flux, and reactive oxygen species (ROS) production has been correlated with ETC driving forces,<sup>54</sup> the increased conductance of the ETC with  $\text{Ca}^{2+}$  levels typical of exercising muscle may suggest a role for  $\text{Ca}^{2+}$  in minimizing ROS production upon the onset of exercise. Indeed, though  $\text{Ca}^{2+}$  given to inhibited mitochondria or in supraphysiologic doses causes an increase in the level of ROS production,<sup>55</sup> control mitochondria produce less ROS from Complexes I and III when given physiological levels of  $\text{Ca}^{2+}$ .<sup>56,57</sup>

Recent advancements in optical absorbance spectroscopy<sup>31</sup> have allowed for measurement of the status of individual complexes of the ETC without the use of artificial electron donors/acceptors or inhibitors and under conditions similar to those typically used in mitochondrial respiration studies. We employed these methods together with the force–flow analyses described above to determine the conductances of individual elements within the ETC. Surprisingly, we found that  $\text{Ca}^{2+}$  activated nearly every step within the ETC (Figure 9), with a 2.2-fold effect on  $L_{\text{CI+III}}$ , a 2.4-fold effect on  $L_{\text{CIVa}}$ , and a 2.2-fold effect on  $L_{\text{CIVb}}$ . Unfortunately, we were unable to measure the redox status of ubiquinone, which precluded the separation of Complexes I and III. However, on the basis of our measurements of the redox status of cyt  $b_{\text{H}}$  and the proposed equilibrium between cyt  $b_{\text{H}}$  and ubiquinone,<sup>58–60</sup> we can predict that the effect of  $\text{Ca}^{2+}$  on  $L_{\text{CI+III}}$  would be shared by both Complex I and Complex III. There have been few other reports of a  $\text{Ca}^{2+}$  stimulation of the ETC. Bender and Kadenbach<sup>61</sup> showed that  $\text{Ca}^{2+}$  rescued the inhibition of Complex IV activity by cAMP in bovine liver mitochondria; however,  $\text{Ca}^{2+}$  had no effect when cAMP was not present and did not directly activate the isolated enzyme. Murphy et al.<sup>15</sup> suggested that the  $\text{Ca}^{2+}$  sensitivity of rat liver mitochondria was largely due to activation of flow through Complex III, but not Complex IV. However, Murphy et al.<sup>15</sup> reported a  $\text{Ca}^{2+}$ -stimulated maximal flux through Complexes III and IV (from ubiquinone to  $\text{O}_2$ ) that was more than twice as high as the flux through Complex IV alone (from TMPD and ascorbate to  $\text{O}_2$ ), suggesting that maximal Complex IV flux was not attained with TMPD and ascorbate as the substrate in that study.

To the best of our knowledge, the current broadband, spectroscopic approach is the first report of  $\text{Ca}^{2+}$  activation of multiple steps within the ETC. This activation of the ETC by  $\text{Ca}^{2+}$  may significantly contribute to the  $\text{Ca}^{2+}$  stimulation of ATP production during exercise. Hogan's lab recently found that a "priming" bout of contractions removed an apparent limitation to flux caused by the ETC at the onset of contractions in an isolated single muscle fiber.<sup>62</sup> These authors speculated that an increase in the mitochondrial  $\text{Ca}^{2+}$  level may have been responsible, at least in part, for the removal of the limitation to flux by the ETC, though  $\text{Ca}^{2+}$  levels were not specifically measured.<sup>62</sup>

**Network Thermodynamic Analysis.** By calculating the conductances for sequential steps within the mitochondrial energy conversion cascade, we are also able to treat the system as a series of resistors in which the resistance of each part is the reciprocal of its conductance. The total resistance of the series of reactions is then equal to the sum of the individual resistances within the system. This approach is similar to network thermodynamic approaches used for modeling multiple reaction steps in a metabolic cascade.<sup>63,64</sup> Further, we can



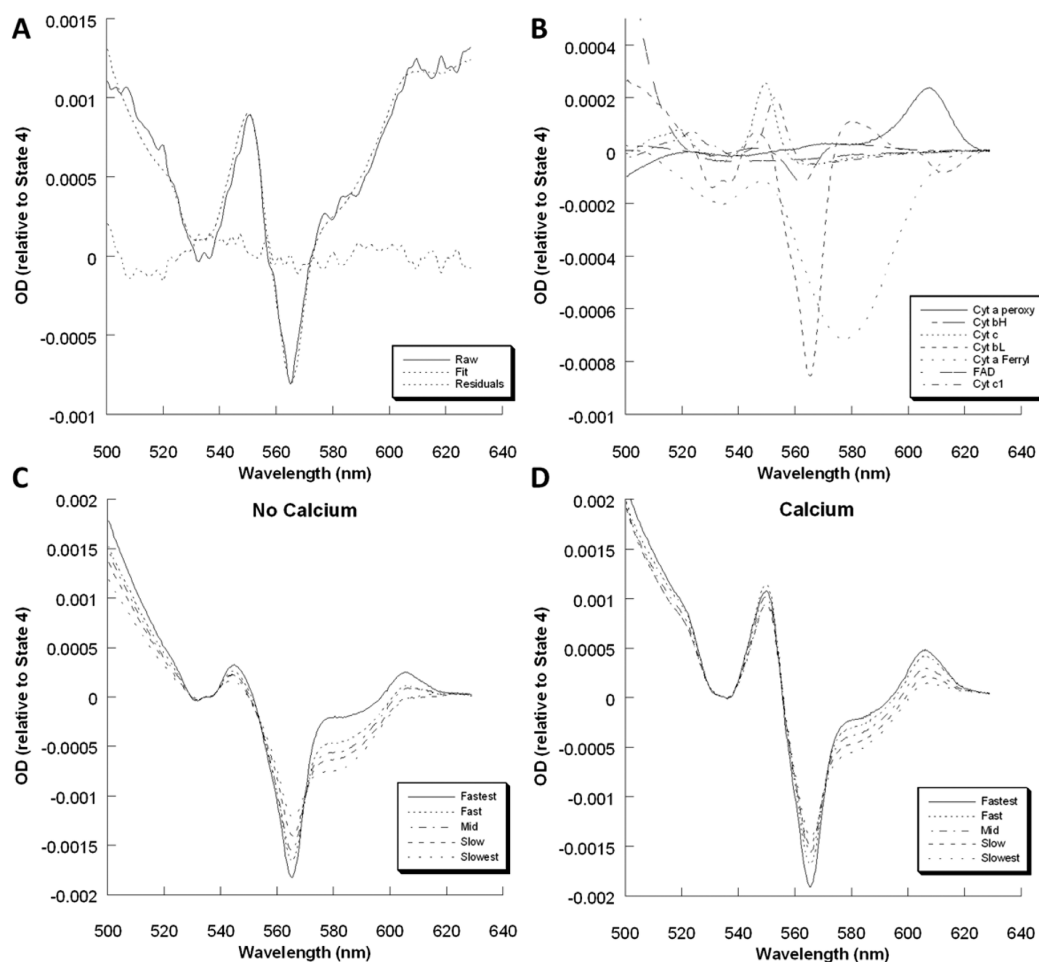


**Figure 7.** Representative spectra and fits for mitochondrial cytochromes. (A) Representative raw, fit, and error residual spectra of a transition from State 4 to intermediate respiration. (B) Individual cytochrome components of the fit spectrum from panel A. (C) Representative fit spectra from a CK clamp experiment without calcium. (D) Representative fit spectra from a CK clamp experiment with calcium.

calculate the resistance of each individual element as a percentage of the total resistance and examine whether  $\text{Ca}^{2+}$  alters the distribution of resistances within the energy conversion elements.  $\text{Ca}^{2+}$  addition resulted in a 1.9-fold decrease in the total resistance to mitochondrial energy conversion as well as a decrease in the resistance of each element (Table 3). However, the distribution of the resistances within the reaction series was altered by  $\text{Ca}^{2+}$ . The ETC contributed 64.8% of the total resistance to flux in the absence of  $\text{Ca}^{2+}$ , while the presence of  $\text{Ca}^{2+}$  reduced the contribution of the ETC to 51.7% of the total resistance to energy conversion. Despite the well-known effects of  $\text{Ca}^{2+}$  on increasing the activity of substrate dehydrogenases,<sup>7,65</sup>  $\text{Ca}^{2+}$  trended toward an increase ( $p = 0.09$ ), not a decrease, in the resistance of the fuel transport/substrate dehydrogenase pathway relative to the other components of mitochondrial energy transfer (Table 3). Thus, while  $\text{Ca}^{2+}$  did activate fuel transport/substrate dehydrogenases [ $L_{\text{fuel/DH}}$  (Table 2)], the effects were relatively greater on downstream pathways. This was not surprising, however, as it was recently pointed out that  $\text{Ca}^{2+}$  stimulation of respiration cannot be explained by activation of dehydrogenases alone.<sup>53</sup>

The data in Table 3 also suggest that Complex IV and Complex V and/or ANT are critical sites of flux control within mitochondria respiring at intermediate rates, as these sites make the greatest contribution to the total mitochondrial resistance

to energy conversion. Complex IV, Complex V, and ANT have each previously been reported to be an important locus of flux control in heart mitochondria,<sup>66–68</sup> though the simulations of Korzeniewski and Mazat<sup>69</sup> suggested that, in skeletal muscle mitochondria, these three sites have little or no flux control during intermediate respiration. However, the hexokinase–ATPase system utilized by Korzeniewski and Mazat assumed 85% of the flux control during intermediate respiration with an additional 8% coming from the proton leak, leaving little room for flux control by any mitochondrial enzyme. The CK energy clamp system used here exerts no flux control itself,<sup>68</sup> thus allowing for greater sensitivity in detecting the relative control of mitochondrial sites over energy conversion.<sup>70</sup>

The observation that multiple steps of oxidative phosphorylation are regulated by  $\text{Ca}^{2+}$  is consistent with previous control strength analyses, using the approach of Kascr and Burns,<sup>71</sup> revealing that the control of oxidative phosphorylation is highly distributed under phosphorylating conditions.<sup>72–74</sup> These studies used inhibitor titrations of different steps in the reaction series to establish if “excessive” activity was present and estimate the control strength of a given step based on the overall flux sensitivity to inhibitor action. These titrations, which did not compensate for changes in reaction driving forces as done here and which relied on the specificity of complex inhibitors, also revealed that Complex IV, ANT, and other steps within the ETC all contribute to the overall rate limitation of

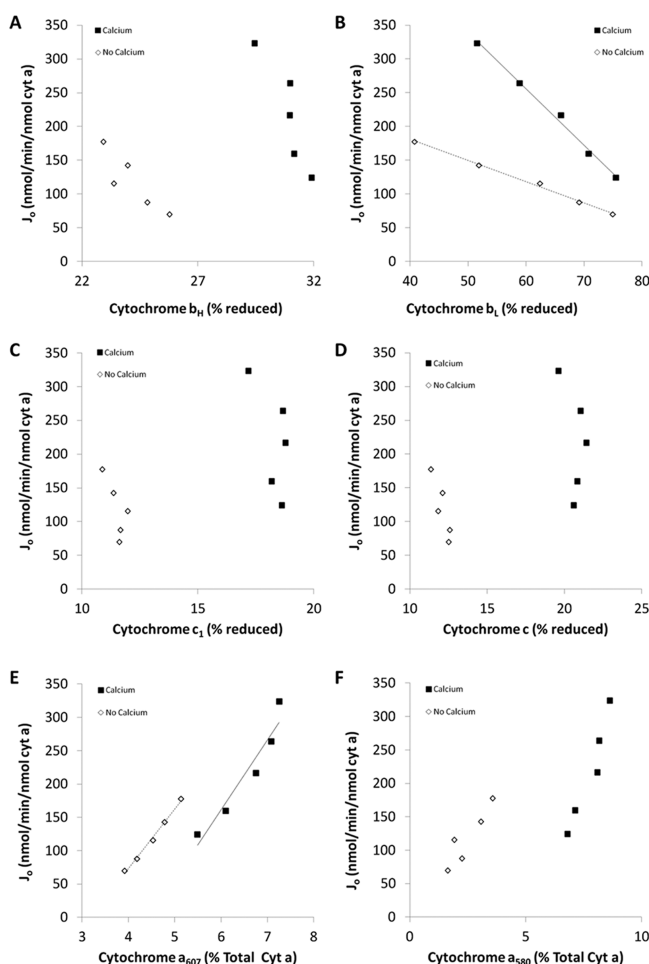


**Figure 8.** Effect of calcium on the kinetic relationship between cytochrome redox state and flux. (A) Relationship between cyt  $b_H$  and  $J_o$  with and without calcium. (B) Relationship between cyt  $b_L$  and  $J_o$  with and without calcium. (C) Relationship between cyt  $c_1$  and  $J_o$  with and without calcium. (D) Relationship between cyt  $c$  and  $J_o$  with and without calcium. (E) Relationship between cyt  $a_{607}$  and  $J_o$  with and without calcium. (F) Relationship between cyt  $a_{580}$  and  $J_o$  with and without calcium. For all panels: (■) calcium and (◇) no calcium. Trend lines are included for relationships with  $r^2$  values of  $>0.8$ .  $n = 4$ . Slopes, regression analyses, and the resultant  $p$  values are listed in Table 2.

State 3 oxidative phosphorylation. In the absence of large changes in metabolite or intermediate concentrations, shared flux control among many sites within the energy conversion process necessitates a coordinated modulation of each site to achieve the large increases in flux observed *in vivo*.<sup>75</sup> This theoretical prediction was bolstered by the *in silico* results of Korzeniewski,<sup>11,76,77</sup> which, using a simplified model of oxidative phosphorylation, suggested that the  $V_{max}$  values of the entire mitochondrial energy conversion process should be modulated by an external signal consistent with notions previously presented by Balaban<sup>10</sup> and Hochachka and Matheson<sup>78</sup> based on experimental data. Although previous cellular and whole tissue studies have found both pyruvate dehydrogenase (PDH) and Complex V to be activated by the onset of contractile work,<sup>49,66,79</sup> experimental evidence of simultaneous, multisite modulation by an external effector has been limited.<sup>6,9,80</sup> The nearly ubiquitous activation across the mitochondrial energy conversion cascade observed here

suggests that  $Ca^{2+}$  may play a role in the stimulation of oxidative phosphorylation *in vivo* contributing to the near metabolic homeostasis observed. However, the molecular mechanism for this effect is yet to be fully elucidated with the exception of a few dehydrogenases.

**Contribution of Conductance and Driving Force to Flux.** The force–flow and network thermodynamic analyses discussed above were conducted under the assumption that energetic flux can be explained by Ohm's law. In other words, the current ( $J_o$ ) must be equal to the voltage ( $\Delta G$ ) multiplied by the conductance ( $L$ ) (eq 6). The linearity displayed in Figures 3, 4, 6, and 9 suggests that this was a valid assumption for nearly all steps within the oxidative phosphorylation cascade. With the establishment of flux as the product of driving force and conductance, we can then determine how much of the increase in flux due to  $Ca^{2+}$  can be attributed to a change in driving force versus a change in conductance.  $Ca^{2+}$  caused an average 2.01-fold increase in  $J_o$  (Figure 3A) upon comparison of mitochondria provided the same extramitochondrial conditions (fuel and  $\Delta G_{ATP}$ ). The driving force for oxidative phosphorylation ( $\Delta G_{NADH} - \Delta G_{ATP}$ ) increased on average by only 1.03-fold with  $Ca^{2+}$  (Figure 6A); consequently, 97% of the increase in  $J_o$  must be explained by an increase in the conductance of this pathway ( $L_{oxphos}$ ). The overall driving force for the ETC ( $\Delta G_{NADH} - \Delta G_{\Delta\psi}$ ) actually decreased by 15% with  $Ca^{2+}$  (Figure 6C), and as a result, the increase in  $L_{ETC}$  can explain the entire  $Ca^{2+}$ -induced increase in flux down this pathway. Within the ETC, 100 and 98% of the greater flux observed with  $Ca^{2+}$  is explained by an increase in the conductances of Complex I–III (Figure 9A) and Complex IV (Figure 9C,D), respectively. Similarly, the driving force for the combined fuel transport and substrate dehydrogenase pathways ( $\Delta G_{fuel} - \Delta G_{NADH}$ ) decreased slightly with  $Ca^{2+}$ , suggesting that a change in conductance, and not driving force, is entirely responsible for the increase in flux observed with  $Ca^{2+}$ . Although the level of NADH and  $\Delta\psi$  merely reflect the balance of their respective production and utilization and do not offer direct insight into the specific location of any conductance changes, similar comparisons of the contribution of driving force versus conductance to the observed increase in flux can also be made for these two energetic intermediates.  $Ca^{2+}$  caused a 4% increase in both NADH and  $\Delta\psi$  (Figure 4); thus, the contribution of these two driving forces to the 2.01-fold increase in  $J_o$  was minimal compared to the associated increases in conductance due to  $Ca^{2+}$ .

Conversely, addition of  $Ca^{2+}$  led to an average 1.25-fold increase in  $\Delta G_{\Delta\psi} - \Delta G_{ATP}$  (Figure 6B); thus, only 76% of the increase in flux through the ATP production and transport reactions can be explained by  $L_{ATPase}$ . The fact that  $\Delta G_{\Delta\psi} - \Delta G_{ATP}$  was also able to explain a significant fraction of the  $Ca^{2+}$ -stimulated flux suggests that this thermodynamic parameter itself may play an important role in flux control. Similarly, the reduction level of cyt  $a_{607}$  (Figure 8e) is reported to be a primary controller of flux through Complex IV.<sup>67</sup> Just as with  $\Delta G_{\Delta\psi} - \Delta G_{ATP}$ , the increase in the reduction level of cyt  $a_{607}$  can explain 54% of the increase in flux through Complex IV due to  $Ca^{2+}$ , leaving 46% to be explained by activation of the enzyme. Moreover, in preliminary experiments in which  $J_o$  was manipulated first by titrating increasing amounts of fuel (push) and subsequently by increasing the PCr/Cr ratio (pull) of the energetic parameters measured here, only  $\Delta G_{\Delta\psi} - \Delta G_{ATP}$  and the reduction level of cyt  $a_{607}$  maintained a positive, linear relationship with  $J_o$  during both the push and pull phases

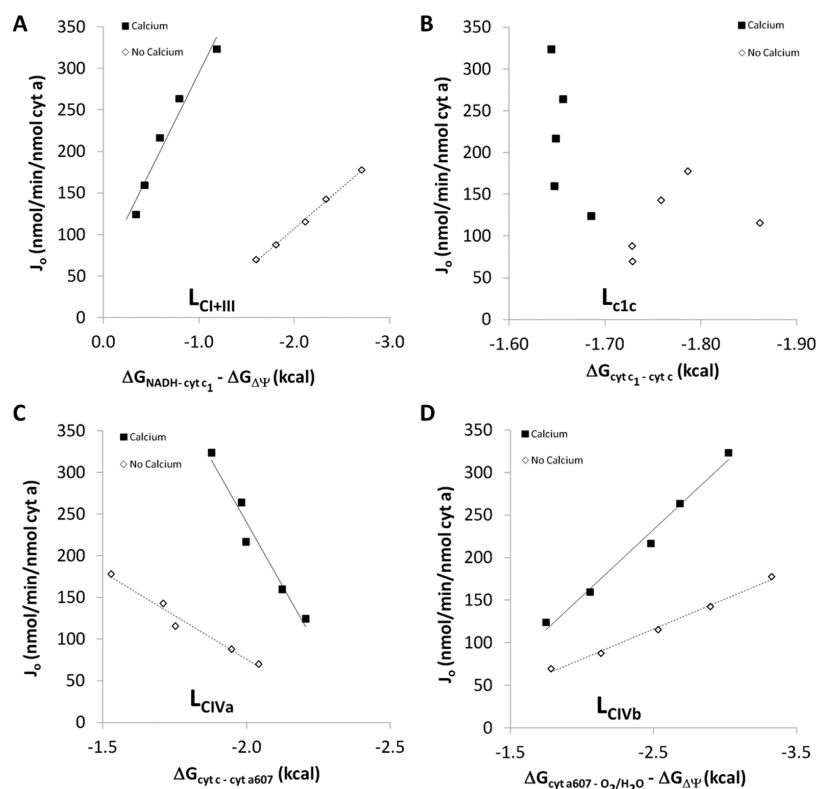


**Figure 9.** Conductances within the electron transport chain. (A) Conductance of electron flux between NADH and cyt  $c_1$  with and without calcium. (B) Conductance of electron flux between cyt  $c_1$  and cyt  $c$  with and without calcium. (C) Conductance of electron flux between cyt  $c$  and cyt  $a_{607}$  with and without calcium. (D) Conductance of electron flux between cyt  $a_{607}$  and  $O_2$  with and without calcium. For all panels: (■) calcium and (◇) no calcium. Trend lines are included for relationships with  $r^2$  values of  $>0.8$ .  $n = 4$ . Slopes, regression analyses, and the resultant  $p$  values are listed in Table 2 for panels A–D as  $L_{C1+III}$ ,  $L_{c1c}$ ,  $L_{CIVa}$ , and  $L_{CIVb}$ , respectively.

**Table 3. Contribution of Each Pathway to the Total Mitochondrial Resistance to Energy Transfer<sup>a</sup>**

	fuel transport/dehydrogenases	Complex I+III	Complex IV	ATP production/transport	total resistance ( $\Omega$ /nmol of cyt $a$ )
no calcium	$10.4 \pm 0.8\%$ (467)	$27.1 \pm 2.4\%$ (1211)	$37.7 \pm 3.3\%$ (1685)	$24.7 \pm 4.0\%$ (1106)	$4471 \pm 558$
calcium	$14.8 \pm 3.2\%$ (345)	$21.2 \pm 2.5\%^b$ (495)	$30.5 \pm 3.6\%^b$ (711)	$29.1 \pm 4.1\%^b$ (678)	$2332 \pm 441^b$

<sup>a</sup>The mitochondrial energy conversion process was considered as a series of resistors in which the total resistance is the sum of the individual parts. Resistance was calculated as the reciprocal of conductance and assuming 1 nmol of  $O_2 = 4 \times 6.02e^{14}$  electrons,  $6.24e^{18}$  electrons = 1 coulomb, and 1 V = 23.062 kcal/mol.  $n = 8$ . <sup>b</sup>Denotes significantly different from the value for no calcium. Values are means  $\pm$  the standard error with mean resistance in ohms per nanomole of cyt  $a$  in parentheses.

**Table 4. Thermodynamic Stoichiometries for Individual Spans of the Electron Transport Chain**

stoichiometry	oxphos span	measured		used	% difference	
		no Ca	Ca		no Ca	Ca
$H^+/e^-$	NADH to cyt $c_1$	$3.9 \pm 0.0$	$3.8 \pm 0.0$	4.0	−2.5	−5.0
	cyt $c_1$ to cyt $c$	$0.1 \pm 0.0$	$0.1 \pm 0.1$	0.0	—	—
	cyt $c$ to cyt $a_{607}$	$0.3 \pm 0.0$	$0.3 \pm 0.0$	0.0	—	—
	cyt $a_{607}$ to $O_2$	$1.1 \pm 0.1$	$1.1 \pm 0.0$	1.0	10.0	10.0
	NADH to $O_2^a$	$5.4 \pm 0.1$	$5.2 \pm 0.1$	5.0	8.0	4.0
	NADH to $O_2^b$	$5.4 \pm 0.1$	$5.3 \pm 0.0$	5.0	8.0	6.0

<sup>a</sup>Measured values are the sum of NADH to cyt  $c_1$ , cyt  $c_1$  to cyt  $c$ , cyt  $c$  to cyt  $a_{607}$ , and cyt  $a_{607}$  to  $O_2$ . <sup>b</sup>Measured values are from NADH to  $O_2$  directly.  $n = 4$ .

(Figures S1 and S2 of the Supporting Information). Thus, these data suggest that  $\Delta G_{\Delta\Psi} - \Delta G_{ATP}$ , the reduction level of cyt  $a_{607}$ , and the conductances through each step all play an important role in determining the rate of mitochondrial energy conversion.

**Extrapolation to *in Vivo* Skeletal Muscle.** The extrapolation of these data to *in vivo* conditions is complicated

by the mitochondrial isolation process, the incubation conditions, and the removal from the local, cellular environment. However, these comparisons are useful in understanding these limitations. The addition of  $Ca^{2+}$  to levels similar to those observed during exercise *in vivo* provided a 2-fold increase in the maximal velocity of mitochondrial energy conversion *in vitro* (Figure 3).  $Ca^{2+}$  has been proposed to play a significant

role in the matching of energy supply with demand in the heart<sup>12,81</sup> where the rate of ATP turnover can increase 5-fold with no change in the cellular energy level.<sup>82</sup> Evidence of a balanced activation of the energy supply and demand pathways in skeletal muscle had been limited to *in silico* models<sup>11,76,77</sup> until recently when Wüst et al.<sup>13</sup> reported that the rapid increase in  $J_o$  observed at the onset of muscle contractions *in vivo* was best described by a model of “parallel activation”. These authors showed that the increase in ADP concentration at the onset of exercise was insufficient to account for the fast increase in  $J_o$  observed; instead, an increase in the apparent  $V_{\max}$  of oxidative phosphorylation was required to explain their results. The ADP concentrations and  $K_m$  values reported for the canine gastrocnemius in the study by Wüst et al.<sup>13</sup> covered the range evaluated here (range of 17–66  $\mu\text{M}$ ;  $K_m = 43 \mu\text{M}$ ); however, they reported an  $\sim 17$ -fold increase in  $J_o$  over this ADP concentration range *in vivo*, whereas we find a 4.2-fold increase in  $J_o$  with the combined effects of ADP and  $\text{Ca}^{2+}$  *in vitro* (Figure 3B). The lower dynamic range *in vitro* is also demonstrated by the respiratory control ratio of  $\sim 15$  (Table 1) when the *in vivo* values have been reported to approach 100.<sup>1</sup> The lower dynamic range of our measures could be due to a lower maximal rate of oxidative phosphorylation or a higher “resting” rate. Combining the measured cyt  $a/a_3$  content of  $11.8 \pm 1.6$  nmol of cyt  $a/\text{g}$  of wet weight for the porcine vastus intermedius with the measured *in vitro*  $J_o$  at  $\sim 66 \mu\text{M}$  ADP [ $259.2 \text{ nmol of O}_2 \text{ min}^{-1} (\text{nmol of cyt } a)^{-1}$ ] approaches the *in vivo* value reported by Wüst et al. [ $\sim 65 \text{ mL of O}_2 (\text{kg of muscle})^{-1} \text{ min}^{-1}$ ], while at  $\sim 17 \mu\text{M}$  ADP without  $\text{Ca}^{2+}$ , the rates were  $15.2$  (*in vitro*) and  $3.8 \text{ mL of O}_2 (\text{kg of muscle})^{-1} \text{ min}^{-1}$  (*in vivo*), suggesting that the maximal rate is similar under both conditions and that the discrepancy primarily resided in the resting rates (note that resting here is defined as  $17 \mu\text{M}$  ADP without  $\text{Ca}^{2+}$ ). The reasons for this may be severalfold. First, to take simultaneous, quantitative measurements of  $J_o$ , NADH, and  $\Delta\Psi$ , we used isolated mitochondria removed from their native, reticular environment. Though these mitochondria were of high purity<sup>21</sup> and functional integrity, it is likely that the isolation process alters mitochondrial function to some degree.<sup>83</sup> Indeed, PDH is reported to be activated after mitochondrial isolation<sup>28,84</sup> and, together with other dehydrogenases, may contribute to a higher resting  $J_o$  *in vitro*. Similar results have been obtained for Complex IV and Complex V, where heart biopsies had 2–4-fold lower activity compared to mitochondria isolated from the same tissue.<sup>49</sup> Second, these studies were performed with an excess of glutamate and malate to ensure there would be no fuel limitations and to help maintain the steady state. This could result in a higher than normal delivery of reducing equivalents and also increase the resting  $J_o$ . Finally, the leak rate may also be enhanced during the highly disruptive mitochondrial isolation process.<sup>83</sup> With these points taken together, the combination of excess substrates, alterations in membrane leaks, and the activation of metabolic enzyme activity by the mitochondrial isolation process is likely to explain much of the increased resting  $J_o$  *in vitro* compared to *in vivo*. However, the resultant lower  $J_o$  dynamic range *in vitro* would be expected to render the mitochondria less sensitive to  $\text{Ca}^{2+}$ ; thus, the results presented here may actually underestimate the effect of  $\text{Ca}^{2+}$  *in vivo*. Indeed, simultaneous measures of mitochondrial  $\Delta\Psi$ , NADH, cytochrome redox state, and phosphorylation potential in the intact functioning muscle should provide a better

understanding of how the mechanisms outlined in isolated mitochondria may be in play *in vivo*.

**Assumptions and Calculations.** The nature of these experiments cannot distinguish between mitochondrial surface and matrix calcium effects. It was assumed that most of these effects are primarily due to changes in matrix calcium based on several factors. First, it has been shown that the matrix  $\text{Ca}^{2+}$  level increases *in vivo* with muscle contraction. Rogers et al.<sup>85</sup> demonstrated using  $\text{Ca}^{2+}$  sensitive bioluminescence probes that the mitochondrial  $\text{Ca}^{2+}$  activity does increase with skeletal muscle contraction in an *in vivo* transgenic mouse. These data support the results of earlier, more invasive studies<sup>86</sup> and confirm the notion that an influx of  $\text{Ca}^{2+}$  into the mitochondrial matrix is occurring in the exercising muscle. Second, as reviewed by Glancy and Balaban,<sup>53</sup> most of the effects of  $\text{Ca}^{2+}$  on mitochondrial metabolism are eliminated by blocking the entry of  $\text{Ca}^{2+}$  into the mitochondrial matrix. Extra-mitochondrial  $\text{Ca}^{2+}$  can impact some mitochondrial transporters, such as aralar<sup>87</sup> that, as part of the malate-aspartate shuttle (MAS), has been shown to play an important role in flux control in brain mitochondria.<sup>88</sup> However, we believe there is little flux control by aralar in skeletal muscle mitochondria as aralar activity is 5-fold higher in mitochondria from skeletal muscle than in mitochondria from brain for any given  $\text{Ca}^{2+}$  concentration.<sup>89</sup> Thus, while  $\text{Ca}^{2+}$  stimulation of aralar may remove a limitation to flux in brain mitochondria, the basal activity of aralar in skeletal muscle mitochondria is likely sufficient as to not impede flux. Moreover, in preliminary experiments, we gave mitochondria G+M and used arsenite to inhibit 2-oxoglutarate dehydrogenase, ensuring that only the mitochondrial components of the MAS were capable of providing NADH to the ETC and that aralar was the primary site of entry of glutamate into the matrix. Under these conditions, State 3  $J_o$  was no different with or without  $\text{Ca}^{2+}$  and was similar to the no  $\text{Ca}^{2+}$  condition without arsenite present (data not shown). These results suggest that the 2-fold activation of  $J_o$  with  $\text{Ca}^{2+}$  as shown in Figure 1 occurred largely through effects beyond those on aralar.

The calculation of the various  $\Delta G$  values reported here requires a number of additional assumptions to be made. The first is the attainment of the fully oxidized and reduced states for each redox pair. For cyt  $c_1$  and cyt  $c$ , we used sodium hydrosulfite to reach full chemical reduction at the end of each experiment. However, we are unable to use this method with NADH because, in addition to the NADH fluorescent enhancement by binding to Complex I,<sup>90</sup> the fluorescent signal is dependent on mitochondrial integrity and is severely disturbed by sodium hydrosulfite. As a result, fully reduced NADH was determined under anoxic conditions and in the presence of  $\text{Ca}^{2+}$  for every experiment. The fully oxidized state for NADH and the cytochromes was determined after the 6 min  $\text{Ca}^{2+}$  depletion and subsequent additions of 10 mM P<sub>i</sub> and 0.13 mM ADP. Under this condition, the fluorescent NADH signal is  $\sim 10\%$  above that of the dark current even without correcting for non-NADH fluorescent background in the mitochondria, suggesting that NADH can be further maximally oxidized by only  $\sim 0$ – $10\%$ . This implied that the primary reducing equivalent source for the cytochromes was highly oxidized under these conditions, supporting our assumption that this was a reasonable estimate of the fully oxidized state of the “downstream” cytochromes. We were unable to measure full chemical (ferricyanide) oxidation in intact mitochondria



because of the disruption of the mitochondrial structure with this agent.

The next step in the  $\Delta G$  calculations involves calculating redox potentials ( $E_h$ ) from percent reduced values (eq 1) and requires a midpoint potential ( $E_m$ ) for each redox pair.  $E_m$  values, especially for the various forms of cyt *a* as well as cyt *c*, are highly variable throughout the literature, and while the choice of  $E_m$  to use for each redox pair does alter the absolute  $\Delta G$  values, the slopes in Figures 4, 6, 8, and 9 do not change regardless of the  $E_m$  chosen. Thus, the  $E_m$  values chosen have no effect on the relative conclusions reached herein with regard to  $\text{Ca}^{2+}$ . The final assumptions made in the  $\Delta G$  calculations are the values to use for the number of electrons transferred ( $n$ ), the relative distance electrons travel across the width of the inner membrane between redox pairs ( $z$ ), the number of protons pumped ( $m$ ), and the P/O ratio ( $p$ ) (eqs 3–5). All  $\Delta G$  calculations were made assuming 1 NADH donated 2 electrons ( $n$ ) yielding 10 protons ( $m$ ) resulting in 2.7 ATP molecules ( $p$ ) from the consumption of  $1/2\text{O}_2$ . The pumping of 4, 4, and 2 protons per 2 electrons passed by Complexes I, III, and IV, respectively, has been widely accepted. Further validation of the values chosen for  $n$ ,  $m$ , and  $z$  and the  $E_m$  values is provided by the measurement of force ratios,<sup>40–42</sup> which provides the value for the number of protons pumped per electron transferred under equilibrium, or static head, conditions. Table 4 shows the close matching between the theoretical and measured stoichiometry values used in the free energy calculations and, perhaps more importantly, shows that there was no difference with the addition of  $\text{Ca}^{2+}$ .

The number of protons required to elicit a 360° rotation of the  $\gamma$  subunit of Complex V and synthesize three molecules of ATP is thought to be determined by the size of the c ring within Complex V.<sup>91</sup> Mammalian Complex V has eight c subunits,<sup>92</sup> thus, the H/ATP ratio is 8/3 or 2.67. However, transport of ATP from the mitochondria also comes at the expense of one proton; thus, the overall H/ATP ratio is 3.67, yielding a P/O ratio of 10/3.67 or 2.7. This value represents the theoretical maximal P/O ratio, as the actual value may be lower because of the contribution of the proton leak. Unfortunately, we did not measure proton leak kinetics here; however, on the basis of the respiratory control ratios reported in Table 1, the contribution of the proton leak in these mitochondria under phosphorylating conditions is likely very low. By assuming that proton leak is 100% of State 4 respiration and 0% at State 3 and utilizing a standard relationship between membrane potential and proton leak, we can estimate that accounting for the proton leak would alter the slopes in Figure 6B by ~10% and have a <5% effect on the no  $\text{Ca}^{2+}$ / $\text{Ca}^{2+}$  ratio between slopes. Further, we do not expect a difference in proton leak between  $\text{Ca}^{2+}$  and no  $\text{Ca}^{2+}$  conditions as  $\text{Ca}^{2+}$  does not alter proton leak kinetics in either heart<sup>80</sup> or skeletal muscle mitochondria<sup>6</sup> oxidizing NAD-linked substrates, and we find no difference in the ADP/O ratio with  $\text{Ca}^{2+}$  in heart mitochondria.<sup>9</sup>

Additionally, we did not attempt to measure the contribution of the pH gradient to the protonmotive force in this study. Lambert and Brand<sup>25</sup> found that increasing the  $\text{P}_i$  concentration lowered the pH gradient in skeletal muscle mitochondria, and extrapolation of their data to 10 mM  $\text{P}_i$  as used here would make the pH gradient nearly zero. Moreover, the use of 15 mM sodium in our medium, and the resultant sodium/proton exchange, would be expected to drive the pH gradient even lower than that observed by Lambert and Brand.<sup>25</sup> In addition, we previously reported that there was no pH gradient

in phosphorylating mitochondria under conditions similar to those used in this study.<sup>23</sup> Finally, Kavanagh et al.<sup>6</sup> reported that the pH gradient did not change across a wide range of respiration rates in skeletal muscle mitochondria given NAD-linked substrates with and without  $\text{Ca}^{2+}$ . Thus, any contribution of the pH gradient could be expected to be the same for all points in the force–flow plots, thereby yielding no effect on the slopes and, therefore, the results reported here.

Initial free energy analyses involving cyt *a* were conducted in a manner similar to those mentioned above where sodium hydrosulfite was used to determine the fully reduced state using the spectral peak observed at 605 nm, redox potential was determined using a published  $E_m$  value,  $\Delta G$  was calculated using the appropriate proton and electron stoichiometries, and these assumptions were validated by the measurement of the force ratios (Table 4). However, as discussed in previous work,<sup>31</sup> closer examination revealed that the spectral peak for cyt *a* in the presence of oxygen was consistently observed at 607 nm and not 605 nm, suggesting that the detected species was the peroxy form of cyt *a*.<sup>31,32</sup> The peroxy form of cyt *a* is just one of several intermediates within the catalytic cycle of Complex IV and is not present in both oxidized and reduced forms as with cytochromes *b* and *c*. Further complicating matters, the maximal occupancy of cyt *a*<sub>607</sub> has been reported to represent only ~30% of the total enzyme,<sup>93,94</sup> suggesting that most of the enzyme complex is in different redox states. These findings bring into question the validity of the assumptions made in the quantification of  $\Delta G_{\text{cyt } a_{607}}$  discussed above. It should be noted that the determination of cyt *a* content in detergent extracts with chemical reducing agents does not suffer from this complication because the entire complex is moved to the fully reduced state. Fortunately, we can use the measurements of  $L_{\text{ETC}}$  and  $L_{\text{CI+CIII}}$  to subtract the conductance of Complex I+III from the conductance of the entire ETC to yield another measurement of the conductance of Complex IV. Using this calculation,  $\text{Ca}^{2+}$  still provides a >2-fold increase in the conductance of Complex IV, and the subsequent calculation of resistances as in Table 3 suggests that Complex IV is still the primary site of resistance in the absence of  $\text{Ca}^{2+}$  and that the relative resistance is reduced upon addition of  $\text{Ca}^{2+}$  (data not shown). Additionally, calculation of the conductance of Complex IV can be done by combining  $L_{\text{CIVa}}$  and  $L_{\text{CIVb}}$  and plotting  $\Delta G_{\text{cyt } c-\text{O}_2/\text{H}_2\text{O}} - \Delta G_{\Delta\psi}$  versus  $J_o$ . Again, this calculation provides similar results with regard to the effect of  $\text{Ca}^{2+}$  on the conductance of Complex IV and its resistance relative to the entire energy conversion cascade. These two calculations, combined with the validity provided by the force ratio measurements, suggest that the interpretations that result from the initial analyses of the effect of  $\text{Ca}^{2+}$  on Complex IV were justified. Moreover, we performed additional analyses on the conductance of electron transfer within Complex IV using a method similar to that of Wikström and Morgan<sup>32</sup> in which the peroxy and ferryl forms of cyt *a* were considered one redox couple and the ferryl and oxidized forms were considered another. These results are displayed in Figure 10 and further suggest that  $\text{Ca}^{2+}$  activates Complex IV by altering the conductance of electron transfer within the catalytic cycle of the enzyme in addition to reducing the contribution of Complex IV to the overall resistance to energy conversion.

$\text{Ca}^{2+}$  has also been shown to induce a spectral shift in heme *a* of Complex IV,<sup>95,96</sup> and it is possible that this confounded our results with respect to the  $\text{Ca}^{2+}$  activation of Complex IV

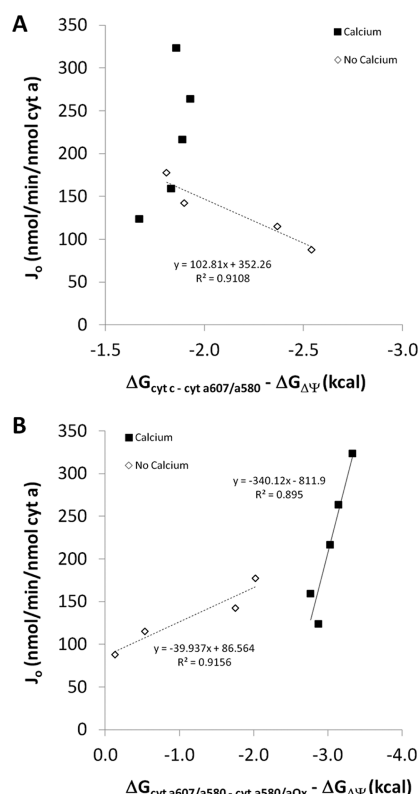


**Figure 10.** Conductance of electron transfer within Complex IV. (A) Conductance of electron flux between the cyt *c* and cyt *a*<sub>607/a580</sub> redox couples. (B) Conductance of electron flux between the cyt *a*<sub>607/a580</sub> and cyt *a*<sub>580/oxidized</sub> redox couples. For all panels: (■) calcium and (◇) no calcium. Trend lines are included for relationships with *r*<sup>2</sup> values of >0.8. *n* = 4.

depicted in Figures 9 and 10. To investigate this possibility, we repeated the experiments of Kirichenko et al.<sup>95</sup> using solubilized porcine mitochondria where cyt *a* was reduced by KCN, ascorbate, and TMPD. Indeed, addition of Ca<sup>2+</sup> induced a red shift of cyt *a* (data not shown). However, the addition of Ca<sup>2+</sup> to intact, respiring mitochondria where Complex IV is more than 90% oxidized induced no such shift in the peak for cyt *a*, suggesting that the observed Ca<sup>2+</sup> activation of Complex IV is not simply due to a Ca<sup>2+</sup>-induced spectral shift.

**Summary.** These data present the first experimental evidence of a systemic modulation of the oxidative phosphorylation cascade by Ca<sup>2+</sup>. This stimulation involves the nearly balanced activation of the entire mitochondrial energy conversion process from the generation of NADH and reduction of oxygen to the formation of ATP from ADP and P<sub>i</sub>. While the mechanism explaining this systemic modulation with Ca<sup>2+</sup> has yet to be elucidated, current evidence suggests that it is not direct Ca<sup>2+</sup> binding as studies of isolated membrane enzymes and submitochondrial particles find no effect of Ca<sup>2+</sup>.<sup>61,97</sup> Thus, it seems likely that Ca<sup>2+</sup> is acting through an as yet unknown coordination of post-translational modifications (PTMs). Whether this involves alterations in supercomplex structure,<sup>98</sup> changes in phosphorylation, multiple PTMs, or other possibilities will be the subject of future work. Additionally, extrapolation of these data to the conditions observed during exercise in skeletal muscle *in vivo* reveals that a significant fraction of the metabolic activation associated with exercise could be attributed to effects of Ca<sup>2+</sup> on oxidative phosphorylation coupled with an increase in ADP concen-

tration, thereby contributing to the metabolic homeostasis of this dynamic tissue.

## ■ ASSOCIATED CONTENT

### Supporting Information

Additional supplemental figures. This material is available free of charge via the Internet at <http://pubs.acs.org>.

## ■ AUTHOR INFORMATION

### Corresponding Author

\*NHLBI, NIH, 10 Center Dr., Room B1D416, Bethesda, MD 20892. E-mail: [glancybp@nhlbi.nih.gov](mailto:glancybp@nhlbi.nih.gov). Phone: (301) 496-2679. Fax: (301) 402-2389.

### Funding

This study was supported by Intramural Funding of the Division of Intramural Research, National Heart, Lung and Blood Institute.

### Notes

The authors declare no competing financial interest.

## ■ REFERENCES

- (1) Weibel, E. R., and Hoppeler, H. (2005) Exercise-induced maximal metabolic rate scales with muscle aerobic capacity. *J. Exp. Biol.* 208, 1635–1644.
- (2) Combs, C. A., Aletras, A. H., and Balaban, R. S. (1999) Effect of muscle action and metabolic strain on oxidative metabolic responses in human skeletal muscle. *J. Appl. Physiol.* 87, 1768–1775.
- (3) Connett, R., and Honig, C. (1989) Regulation of VO<sub>2</sub> in red muscle: Do current biochemical hypotheses fit *in vivo* data. *Am. J. Physiol.* 256, R898–R906.
- (4) Kushmerick, M., Meyer, R., and Brown, T. (1992) Regulation of oxygen consumption in fast and slow twitch muscle. *Am. J. Physiol.* 263, C598–C606.
- (5) Johnston, J. D., and Brand, M. D. (1987) Stimulation of the respiration rate of rat liver mitochondria by sub-micromolar concentrations of extramitochondrial Ca<sup>2+</sup>. *Biochem. J.* 245, 217–222.
- (6) Kavanagh, N. I., Ainscow, E. K., and Brand, M. D. (2000) Calcium regulation of oxidative phosphorylation in rat skeletal muscle mitochondria. *Biochim. Biophys. Acta* 1457, 57–70.
- (7) McCormack, J. G., Halestrap, A. P., and Denton, R. M. (1990) Role of calcium ions in regulation of mammalian intramitochondrial metabolism. *Physiol. Rev.* 70, 391–425.
- (8) Panov, A. V., and Scaduto, R. C., Jr. (1996) Substrate specific effects of calcium on metabolism of rat heart mitochondria. *Am. J. Physiol.* 270, H1398–H1406.
- (9) Territo, P. R., Mootha, V. K., French, S. A., and Balaban, R. S. (2000) Ca<sup>2+</sup> activation of heart mitochondrial oxidative phosphorylation: Role of the F<sub>0</sub>/F<sub>1</sub>-ATPase. *Am. J. Physiol.* 278, C423–C435.
- (10) Balaban, R. S. (1990) Regulation of oxidative phosphorylation in the mammalian cell. *Am. J. Physiol.* 258, C377–C389.
- (11) Korzeniewski, B. (2007) Regulation of oxidative phosphorylation through parallel activation. *Biophys. Chem.* 129, 93–110.
- (12) Balaban, R. S., Bose, S., French, S. A., and Territo, P. R. (2003) Role of calcium in metabolic signaling between cardiac sarcoplasmic reticulum and mitochondria *in vitro*. *Am. J. Physiol.* 284, C285–C293.
- (13) Wust, R. C., Grassi, B., Hogan, M. C., Howlett, R. A., Gladden, L. B., and Rossiter, H. B. (2011) Kinetic control of oxygen consumption during contractions in self-perfused skeletal muscle. *J. Physiol.* 589, 3995–4009.
- (14) McCormack, J. G., and Denton, R. M. (1980) Role of calcium ions in the regulation of intramitochondrial metabolism. Properties of the Ca<sup>2+</sup>-sensitive dehydrogenases within intact uncoupled mitochondria from the white and brown adipose tissue of the rat. *Biochem. J.* 190, 95–105.
- (15) Murphy, A. N., Kelleher, J. K., and Fiskum, G. (1990) Submicromolar Ca<sup>2+</sup> regulates phosphorylating respiration by normal

rat liver and AS-30D hepatoma mitochondria by different mechanisms. *J. Biol. Chem.* 265, 10527–10534.

(16) Martin, C., Dubouchaud, H., Mosoni, L., Chardigny, J. M., Oudot, A., Fontaine, E., Vergely, C., Kerié, C., Rochette, L., Leverve, X., and Demaison, L. (2007) Abnormalities of mitochondrial functioning can partly explain the metabolic disorders encountered in sarcopenic gastrocnemius. *Aging Cell* 6, 165–177.

(17) Carroll, S. L., Klein, M. G., and Schneider, M. F. (1997) Decay of calcium transients after electrical stimulation in rat fast- and slow-twitch skeletal muscle fibres. *J. Physiol.* 501, 573–588.

(18) Westerblad, H., and Allen, D. G. (1991) Changes of myoplasmic calcium concentration during fatigue in single mouse muscle fibers. *J. Gen. Physiol.* 98, 615–635.

(19) Westerblad, H., Duty, S., and Allen, D. G. (1993) Intracellular calcium concentration during low-frequency fatigue in isolated single fibers of mouse skeletal muscle. *J. Appl. Physiol.* 75, 382–388.

(20) Moreno-Sanchez, R., Hogue, B. A., and Hansford, R. G. (1990) Influence of NAD-linked dehydrogenase activity on flux through oxidative phosphorylation. *Biochem. J.* 268, 421–428.

(21) Glancy, B., and Balaban, R. S. (2011) Protein composition and function of red and white skeletal muscle mitochondria. *Am. J. Physiol.* 300, C1280–C1290.

(22) Balaban, R. S., Mootha, V. K., and Arai, A. (1996) Spectroscopic determination of cytochrome c oxidase content in tissues containing myoglobin or hemoglobin. *Anal. Biochem.* 237, 274–278.

(23) Bose, S., French, S., Evans, F. J., Joubert, F., and Balaban, R. S. (2003) Metabolic network control of oxidative phosphorylation: Multiple roles of inorganic phosphate. *J. Biol. Chem.* 278, 39155–39165.

(24) Rasmussen, H. N., and Rasmussen, U. F. (2003) Oxygen solubilities of media used in electrochemical respiration measurements. *Anal. Biochem.* 319, 105–113.

(25) Lambert, A. J., and Brand, M. D. (2004) Superoxide production by NADH:ubiquinone oxidoreductase (complex I) depends on the pH gradient across the mitochondrial inner membrane. *Biochem. J.* 382, 511–517.

(26) Fabiato, A., and Fabiato, F. (1979) Calculator programs for computing the composition of the solutions containing multiple metals and ligands used for experiments in skinned muscle cells. *J. Physiol. (Paris)* 75, 463–505.

(27) Reitz, F. B., and Pollack, G. H. (2003) Labview virtual instruments for calcium buffer calculations. *Computer Methods and Programs in Biomedicine* 70, 61–69.

(28) Messer, J. I., Jackman, M. R., and Willis, W. T. (2004) Pyruvate and citric acid cycle carbon requirements in isolated skeletal muscle mitochondria. *Am. J. Physiol.* 286, C565–C572.

(29) Lefort, N., Glancy, B., Bowen, B., Willis, W. T., Bailowitz, Z., De Filippis, E. A., Brophy, C., Meyer, C., Hojlund, K., Yi, Z., and Mandarino, L. J. (2010) Increased reactive oxygen species production and lower abundance of complex I subunits and carnitine palmitoyltransferase 1B protein despite normal mitochondrial respiration in insulin-resistant human skeletal muscle. *Diabetes* 59, 2444–2452.

(30) Teague, W. E., Jr., and Dobson, G. P. (1992) Effect of temperature on the creatine kinase equilibrium. *J. Biol. Chem.* 267, 14084–14093.

(31) Chess, D., Billings, E., Covian, R., Glancy, B., French, S., Taylor, J., Murphy, E., and Balaban, R. S. (2013) Optical spectroscopy of mitochondrial oxidative phosphorylation complexes using an integrating sphere: Analysis of steady state reducing equivalent distributions. Submitted for publication.

(32) Wikstrom, M., and Morgan, J. E. (1992) The dioxygen cycle. Spectral, kinetic, and thermodynamic characteristics of ferryl and peroxy intermediates observed by reversal of the cytochrome oxidase reaction. *J. Biol. Chem.* 267, 10266–10273.

(33) Proshlyakov, D. A., Pressler, M. A., and Babcock, G. T. (1998) Dioxygen activation and bond cleavage by mixed-valence cytochrome c oxidase. *Proc. Natl. Acad. Sci. U.S.A.* 95, 8020–8025.

(34) Wikstrom, M., and Verkhovsky, M. I. (2007) Mechanism and energetics of proton translocation by the respiratory heme-copper oxidases. *Biochim. Biophys. Acta* 1767, 1200–1214.

(35) Kim, Y. C., Wikstrom, M., and Hummer, G. (2009) Kinetic gating of the proton pump in cytochrome c oxidase. *Proc. Natl. Acad. Sci. U.S.A.* 106, 13707–13712.

(36) Tiesjema, R. H., Muijsers, A. O., and van Gelder, B. F. (1973) Biochemical and biophysical studies on cytochrome c oxidase. X. Spectral and potentiometric properties of the hemes and coppers. *Biochim. Biophys. Acta* 305, 19–28.

(37) Muijsers, A. O., Tiesjema, R. H., Henderson, R. W., and Van Gelder, B. F. (1972) Biochemical and biophysical studies on cytochrome aa 3. VII. The effect of cytochrome c on the oxidation-reduction potential of isolated cytochrome aa 3. *Biochim. Biophys. Acta* 267, 216–221.

(38) Onsager, L. (1931) Reciprocal relations in irreversible processes. II. *Phys. Rev.* 38, 2265–2279.

(39) Onsager, L. (1931) Reciprocal relations in irreversible processes. I. *Phys. Rev.* 37, 405–426.

(40) Brown, G. C., and Brand, M. D. (1985) Thermodynamic control of electron flux through mitochondrial cytochrome bc<sub>1</sub> complex. *Biochem. J.* 225, 399–405.

(41) Brown, G. C., and Brand, M. D. (1988) Proton/electron stoichiometry of mitochondrial complex I estimated from the equilibrium thermodynamic force ratio. *Biochem. J.* 252, 473–479.

(42) Lemasters, J. J. (1984) The ATP-to-oxygen stoichiometries of oxidative phosphorylation by rat liver mitochondria. An analysis of ADP-induced oxygen jumps by linear nonequilibrium thermodynamics. *J. Biol. Chem.* 259, 13123–13130.

(43) Hughes, B. P., and Barritt, G. J. (1978) Effects of glucagon and N<sup>6</sup>O<sub>2</sub>'-dibutyladenosine 3':5'-cyclic monophosphate on calcium transport in isolated rat liver mitochondria. *Biochem. J.* 176, 295–304.

(44) Carafoli, E., and Lehninger, A. L. (1971) A survey of the interaction of calcium ions with mitochondria from different tissues and species. *Biochem. J.* 122, 681–690.

(45) Territo, P. R., French, S. A., Dunleavy, M. C., Evans, F. J., and Balaban, R. S. (2001) Calcium activation of heart mitochondrial oxidative phosphorylation: Rapid kinetics of mVO<sub>2</sub>, NADH, and light scattering. *J. Biol. Chem.* 276, 2586–2599.

(46) Glancy, B., Barstow, T., and Willis, W. T. (2008) Linear relation between time constant of oxygen uptake kinetics, total creatine, and mitochondrial content in vitro. *Am. J. Physiol.* 294, C79–C87.

(47) Kushmerick, M. J., Meyer, R. A., and Brown, T. R. (1992) Regulation of oxygen consumption in fast- and slow-twitch muscle. *Am. J. Physiol.* 263, C598–C606.

(48) Ryschon, T. W., Fowler, M. D., Wysong, R. E., Anthony, A., and Balaban, R. S. (1997) Efficiency of human skeletal muscle in vivo: Comparison of isometric, concentric, and eccentric muscle action. *J. Appl. Physiol.* 83, 867–874.

(49) Phillips, D., Covian, R., Aponte, A. M., Glancy, B., Taylor, J. F., Chess, D., and Balaban, R. S. (2012) Regulation of oxidative phosphorylation complex activity: Effects of tissue-specific metabolic stress within an allometric series and acute changes in workload. *Am. J. Physiol.* 302, R1034–R1048.

(50) Turner, P. R., Westwood, T., Regen, C. M., and Steinhardt, R. A. (1988) Increased protein degradation results from elevated free calcium levels found in muscle from mdx mice. *Nature* 335, 735–738.

(51) Jones, A. M., Wilkerson, D. P., and Fulford, J. (2009) Influence of dietary creatine supplementation on muscle phosphocreatine kinetics during knee-extensor exercise in humans. *Am. J. Physiol.* 296, R1078–R1087.

(52) Kemp, G. J., Taylor, D. J., and Radda, G. K. (1993) Control of phosphocreatine resynthesis during recovery from exercise in human skeletal muscle. *NMR Biomed.* 6, 66–72.

(53) Glancy, B., and Balaban, R. S. (2012) Role of mitochondrial Ca<sup>2+</sup> in the regulation of cellular energetics. *Biochemistry* 51, 2959–2973.



- (54) Starkov, A. A., and Fiskum, G. (2003) Regulation of brain mitochondrial H<sub>2</sub>O<sub>2</sub> production by membrane potential and NAD(P)H redox state. *J. Neurochem.* 86, 1101–1107.
- (55) Hopper, R. K., Carroll, S., Aponte, A. M., Johnson, D. T., French, S., Shen, R. F., Witzmann, F. A., Harris, R. A., and Balaban, R. S. (2006) Mitochondrial matrix phosphoproteome: Effect of extra mitochondrial calcium. *Biochemistry* 45, 2524–2536.
- (56) Brookes, P. S., Yoon, Y., Robotham, J. L., Anders, M. W., and Sheu, S. S. (2004) Calcium, ATP, and ROS: A mitochondrial love-hate triangle. *Am. J. Physiol.* 287, C817–C833.
- (57) Starkov, A. A., Polster, B. M., and Fiskum, G. (2002) Regulation of hydrogen peroxide production by brain mitochondria by calcium and Bax. *J. Neurochem.* 83, 220–228.
- (58) Covian, R., and Trumpower, B. L. (2008) The dimeric structure of the cytochrome bc<sub>1</sub> complex prevents center P inhibition by reverse reactions at center N. *Biochim. Biophys. Acta* 1777, 1044–1052.
- (59) Covian, R., Zwicker, K., Rotsaert, F. A., and Trumpower, B. L. (2007) Asymmetric and redox-specific binding of quinone and quinol at center N of the dimeric yeast cytochrome bc<sub>1</sub> complex. Consequences for semiquinone stabilization. *J. Biol. Chem.* 282, 24198–24208.
- (60) Kim, N., Ripple, M. O., and Springett, R. (2012) Measurement of the mitochondrial membrane potential and pH gradient from the redox poise of the hemes of the bc<sub>1</sub> complex. *Biophys. J.* 102, 1194–1203.
- (61) Bender, E., and Kadenbach, B. (2000) The allosteric ATP-inhibition of cytochrome c oxidase activity is reversibly switched on by cAMP-dependent phosphorylation. *FEBS Lett.* 466, 130–134.
- (62) Gandra, P. G., Nogueira, L., and Hogan, M. C. (2012) Mitochondrial activation at the onset of contractions in isolated myofibers during successive contractile periods. *J. Physiol.* 590, 3597–3609.
- (63) Kummel, A., Panke, S., and Heinemann, M. (2006) Systematic assignment of thermodynamic constraints in metabolic network models. *BMC Bioinf.* 7, 512.
- (64) Oster, G. F., Perelson, A. S., and Katchalsky, A. (1973) Network thermodynamics: Dynamic modelling of biophysical systems. *Q. Rev. Biophys.* 6, 1–134.
- (65) Wan, B., LaNoue, K. F., Cheung, J. Y., and Scaduto, R. C., Jr. (1989) Regulation of citric acid cycle by calcium. *J. Biol. Chem.* 264, 13430–13439.
- (66) Harris, D., and Das, A. (1991) Control of mitochondrial ATP synthesis in the heart. *Biochem. J.* 280, 561–573.
- (67) Wilson, D. F., Owen, C. S., and Holian, A. (1977) Control of mitochondrial respiration: A quantitative evaluation of the roles of cytochrome c and oxygen. *Arch. Biochem. Biophys.* 182, 749–762.
- (68) Kholodenko, B., Zilinskiene, V., Borutaite, V., Ivanoviene, L., Toleikis, A., and Praskevicius, A. (1987) The role of adenine nucleotide translocators in regulation of oxidative phosphorylation in heart mitochondria. *FEBS Lett.* 223, 247–250.
- (69) Korzeniewski, B., and Mazat, J. P. (1996) Theoretical studies on the control of oxidative phosphorylation in muscle mitochondria: Application to mitochondrial deficiencies. *Biochem. J.* 319 (Part 1), 143–148.
- (70) Davis, E., and Davis Van-Thienen, W. (1984) Rate control of phosphorylation-coupled respiration by rat liver mitochondria. *Arch. Biochem. Biophys.* 233, 573–581.
- (71) Kacser, H., and Burns, J. A. (1973) The control of flux. *Symp. Soc. Exp. Biol.* 27, 65–104.
- (72) Groen, A. K., Wanders, R. J., Westerhoff, H. V., van der Meer, R., and Tager, J. M. (1982) Quantification of the contribution of various steps to the control of mitochondrial respiration. *J. Biol. Chem.* 257, 2754–2757.
- (73) Tager, J. M., Groen, A. K., Wanders, R. J., Duszyński, J., Westerhoff, H. V., and Vervoorn, R. C. (1983) Control of mitochondrial respiration. *Biochem. Soc. Trans.* 11, 40–43.
- (74) Rossignol, R., Letellier, T., Malgat, M., Rocher, C., and Mazat, J. P. (2000) Tissue variation in the control of oxidative phosphorylation: Implication for mitochondrial diseases. *Biochem. J.* 347 (Part 1), 45–53.
- (75) Fell, D. A., and Thomas, S. (1995) Physiological control of metabolic flux: The requirement for multisite modulation. *Biochem. J.* 311 (Part 1), 35–39.
- (76) Korzeniewski, B. (1998) Regulation of ATP supply during muscle contraction: Theoretical studies. *Biochem. J.* 330 (Part 3), 1189–1195.
- (77) Korzeniewski, B. (2000) Regulation of ATP supply in mammalian skeletal muscle during resting state → intensive work transition. *Biophys. Chem.* 83, 19–34.
- (78) Hochachka, P. W., and Matheson, G. O. (1992) Regulating ATP turnover rates over broad dynamic work ranges in skeletal muscles. *J. Appl. Physiol.* 73, 1697–1703.
- (79) Hagg, S. A., Taylor, S. I., and Ruberman, N. B. (1976) Glucose metabolism in perfused skeletal muscle. Pyruvate dehydrogenase activity in starvation, diabetes and exercise. *Biochem. J.* 158, 203–210.
- (80) Mildaziene, V., Baniene, R., Nauciene, Z., Marcinkeviciute, A., Morkuniene, R., Borutaite, V., Kholodenko, B., and Brown, G. C. (1996) Ca<sup>2+</sup> stimulates both the respiratory and phosphorylation subsystems in rat heart mitochondria. *Biochem. J.* 320 (Part 1), 329–334.
- (81) Balaban, R. S. (2002) Cardiac energy metabolism homeostasis: Role of cytosolic calcium. *J. Mol. Cell. Cardiol.* 34, 1259–1271.
- (82) Balaban, R. S., Kantor, H. L., Katz, L. A., and Briggs, R. W. (1986) Relation between work and phosphate metabolite in the in vivo paced mammalian heart. *Science* 232, 1121–1123.
- (83) Picard, M., Taivassalo, T., Ritchie, D., Wright, K. J., Thomas, M. M., Romestaing, C., and Hepple, R. T. (2011) Mitochondrial structure and function are disrupted by standard isolation methods. *PLoS One* 6, e18317.
- (84) Kerbey, A. L., Randle, P. J., Cooper, R. H., Whitehouse, S., Pask, H. T., and Denton, R. M. (1976) Regulation of pyruvate dehydrogenase in rat heart. Mechanism of regulation of proportions of dephosphorylated and phosphorylated enzyme by oxidation of fatty acids and ketone bodies and of effects of diabetes: Role of coenzyme A, acetyl-coenzyme A and reduced and oxidized nicotinamide-adenine dinucleotide. *Biochem. J.* 154, 327–348.
- (85) Rogers, K. L., Picaud, S., Roncali, E., Boisgard, R., Colasante, C., Stinnakre, J., Tavittan, B., and Brulet, P. (2007) Non-invasive in vivo imaging of calcium signaling in mice. *PLoS One* 2, e974.
- (86) Rudolf, R., Mongillo, M., Magalhaes, P. J., and Pozzan, T. (2004) In vivo monitoring of Ca<sup>2+</sup> uptake into mitochondria of mouse skeletal muscle during contraction. *J. Cell Biol.* 166, 527–536.
- (87) Satrustegui, J., Pardo, B., and Del Arco, A. (2007) Mitochondrial transporters as novel targets for intracellular calcium signaling. *Physiol. Rev.* 87, 29–67.
- (88) Gellerich, F. N., Gizatullina, Z., Trumbekaitė, S., Korzeniewski, B., Gaynutdinov, T., Seppet, E., Vielhaber, S., Heinze, H. J., and Striggow, F. (2012) Cytosolic Ca<sup>2+</sup> regulates the energization of isolated brain mitochondria by formation of pyruvate through the malate-aspartate shuttle. *Biochem. J.* 443, 747–755.
- (89) Contreras, L., Gomez-Puertas, P., Iijima, M., Kobayashi, K., Saheki, T., and Satrustegui, J. (2007) Ca<sup>2+</sup> Activation kinetics of the two aspartate-glutamate mitochondrial carriers, aralar and citrin: Role in the heart malate-aspartate NADH shuttle. *J. Biol. Chem.* 282, 7098–7106.
- (90) Blinova, K., Levine, R. L., Boja, E. S., Griffiths, G. L., Shi, Z. D., Ruddy, B., and Balaban, R. S. (2008) Mitochondrial NADH fluorescence is enhanced by complex I binding. *Biochemistry* 47, 9636–9645.
- (91) Ferguson, S. J. (2010) ATP synthase: From sequence to ring size to the P/O ratio. *Proc. Natl. Acad. Sci. U.S.A.* 107, 16755–16756.
- (92) Watt, I. N., Montgomery, M. G., Runswick, M. J., Leslie, A. G., and Walker, J. E. (2010) Bioenergetic cost of making an adenosine triphosphate molecule in animal mitochondria. *Proc. Natl. Acad. Sci. U.S.A.* 107, 16823–16827.
- (93) Proshlyakov, D. A., Ogura, T., Shinzawa-Itoh, K., Yoshikawa, S., Appelman, E. H., and Kitagawa, T. (1994) Selective resonance Raman



observation of the “607 nm” form generated in the reaction of oxidized cytochrome c oxidase with hydrogen peroxide. *J. Biol. Chem.* 269, 29385–29388.

(94) Proshlyakov, D. A., Ogura, T., Shinzawa-Itoh, K., Yoshikawa, S., and Kitagawa, T. (1996) Microcirculating system for simultaneous determination of Raman and absorption spectra of enzymatic reaction intermediates and its application to the reaction of cytochrome c oxidase with hydrogen peroxide. *Biochemistry* 35, 76–82.

(95) Kirichenko, A., Vygodina, T., Mkrtchyan, H. M., and Konstantinov, A. (1998) Specific cation binding site in mammalian cytochrome oxidase. *FEBS Lett.* 423, 329–333.

(96) Wikstrom, M., and Saari, H. (1975) A spectral shift in cytochrome a induced by calcium ions. *Biochim. Biophys. Acta* 408, 170–179.

(97) Panov, A. V., and Scaduto, R. C., Jr. (1995) Influence of calcium on NADH and succinate oxidation by rat heart submitochondrial particles. *Arch. Biochem. Biophys.* 316, 815–820.

(98) Lenaz, G., and Genova, M. L. (2009) Structural and functional organization of the mitochondrial respiratory chain: A dynamic super-assembly. *Int. J. Biochem. Cell Biol.* 41, 1750–1772.